In-depth synthetic, physicochemical and *in vitro* biological investigation of a new ternary V(IV) anti-oxidant material based on curcumin.

E. Halevas,[a,g] T.A. Papadopoulos,[b] C.H. Swanson,[b] G.C. Smith,[b] A. Hatzidimitriou,[c] G. Katsipis,[d] A. Pantazaki,[d] I. Sanakis,[e] G. Mitrikas,[e] K. Ypsilantis,[f] G. Litsardakis,[g] A. Salifoglou[a*]

[*] Author to whom correspondence should be addressed.
Tel: +30-2310-996-179 Fax: +30-2310-996-196 E-mail: salif@auth.gr

[a] Laboratory of Inorganic Chemistry and Advanced Materials, Department of Chemical Engineering, Aristotle University of Thessaloniki, Thessaloniki 54124, Greece
[b] Department of Natural Sciences, Thornton Science Park, University of Chester, Chester, CH3 4NU, UK
[c] Laboratory of Inorganic Chemistry, Department of Chemistry, Aristotle University of Thessaloniki, Thessaloniki 54124, Greece
[d] Laboratory of Biochemistry, Department of Chemistry, Aristotle University of Thessaloniki, Thessaloniki54124, Greece
[e] Institute of Nanoscience and Nanotechnology, N.C.S.R. "Demokritos", Aghia Paraskevi 15310, Attiki, Greece
[f] Department of Chemistry, University of Ioannina, Ioannina 45110, Greece
[g] Laboratory of Materials for Electrotechnics, Department of Electrical and Computer Engineering, Aristotle University of Thessaloniki, Thessaloniki 54124, Greece

Abstract

Curcumin is a natural product with a broad spectrum of beneficial properties relating to pharmaceutical applications, extending from traditional remedies to modern cosmetics. The biological activity of such pigments, however, is limited by their solubility and bioavailability, thereby necessitating new ways of achieving optimal tissue cellular response and efficacy as drugs. Metal ion complexation provides a significant route toward improvement of curcumin stability and biological activity, with vanadium being a representative such metal ion, known for its presence in biological systems and its exogenous biological activity in potential pharmaceuticals. Driven by the need to optimally increase curcumin bioavailability and bio-activity through complexation, synthetic efforts were launched to seek out stable species, ultimately leading to the synthesis and isolation of a new ternary V(IV)-curcumin-(2,2'-bipyridine) complex. Physicochemical characterization (elemental analysis, FT-IR, TGA, UV-Visible, NMR, ESI-MS, Fluorescence, X-rays) portrayed the solid-state and solution properties of the ternary complex. Pulsed EPR spectroscopy, in frozen solutions, suggested the presence of two species, cis- and trans-conformers. DFT calculations revealed the salient features and energetics of the two conformers, thereby complementing EPR spectroscopy. The well-described profile of the vanadium species led to its *in vitro* biological investigation involving toxicity, cell metabolism inhibition in cultures of *S. cerevisiae*, ROS-suppressing capacity, lipid peroxidation, and plasmid DNA degradation. A multitude of bio-assays and methodologies in comparison to free curcumin, showed that it exhibits its antioxidant potential in a concentration-dependent fashion, thereby formulating a bioreactivity pro-

file supporting development of new potentially efficient hybrid vanado-pharmaceuticals, targeting (extra)intra-cellular processes under (patho)physiological conditions.

Keywords: Vanadium-curcumin complex, crystal structure and DFT calculations, ROS-suppression, cell metabolism inhibition and DNA degradation, bioreactivity profile and antioxidant agent, hybrid metallo-pharmaceutical.

1. Introduction

Curcumin (diferuloylmethane) is a well-known natural pigment with good stability and low toxicity, the metal coordination chemistry of which has been only partially explored [**1-4**]**.** It is obtained from the rhizomes of the traditional herbal remedy and dietary Indian spice turmeric (*Curcuma longa Linn.*) [**5,6**]**.** It is used in cosmetics, spices, and traditional medicines, particularly in the Orient. As an organic physiological substrate, curcumin shows good optical and electrical properties, owing to the symmetric structure containing a β-diketone moiety and an extensive π-conjugation system in polar media [**7,8**]**.**

Systematic investigations of curcumin reveal a wide spectrum of beneficial properties, exemplifying antioxidant, anti-inflammatory, antimicrobial, and anticancer activities [**9-14**]. Curcumin protects neurons against amyloid-β (Aβ) peptide toxicity, due to its selective binding to amyloid plaques, as already proven through experiments on transgenic mouse models in Alzheimer's disease (AD) [**15,16**]. It is also known to exhibit photo-activated cytotoxicity by inducing apoptosis in cancer cells, comparable to the FDA-approved photodynamic therapy (PDT) drug Photofrin® [**17-20**]. Furthermore, the green emission of curcumin is used in cellular imaging [**21**].

Curcumin exists as keto-enol tautomers (**Scheme 1**), being present predominantly in the keto form in acidic and neutral solutions, with the enol tautomer exhibiting stability in alkaline media. It is safe even at high doses [**22,23**], as shown in animal and human trials, but its effectiveness in clinical applications is limited due to low solubility, poor bioavailability in aqueous media,and hydrolytic instability under physiological conditions [**24-26**]. The main reasons for its poor bioavailability are low absorption, rapid metabolism, and fast systemic elimination from the biological system(s) [**27**]. Hence, despite its efficacy and safety, curcumin has not yet been granted approval as a therapeutic agent.

Several methods have been applied to improve stability and bioavailability of curcumin, including a) addition of piperine as an adjuvant, in order to block the metabolic pathways of curcumin, b) encapsulation in nanoparticles, liposomes, micelles, or phospholipid complexes, c) concomitant administration of quercetin, lecithin, eugenol, genistein, terpinol, etc. [**28**], and d) addition of rubusoside [**29**], or complexation with phosphatidyl choline [**30**].

In view of the wide spectrum of pharmacological properties of curcumin [**31,32**] the investigation of its coordination chemistry with metal ionsemerges as an appealing prospect that may render that physiological agent soluble and bioavailable, thus leading to its employment in diagnostic or therapeutic applications. To

that end, it has been proven that complexation of curcumin to an oxophilic metal ion via the β-diketone moiety renders curcumin hydrolytically stable [**33-35**].

Vanadium has been known to exhibit a wide spectrum of reactivities at the cellular level, with targets eliciting interactions and/or interactions sought out in the framework of human (patho)physiologies [**36**]. From Diabetes mellitus to various forms of cancer, appropriate configuration of the vanadium coordination sphere led to its employment as a competent hybrid metallo-agent, ultimately delivering its biological potential [**37**,**38**]. In view of such reactivity on behalf of vanadium and the associated biological potential of curcumin as an antioxidant natural product, research was launched in our lab to probe into an appropriately configured vanadium-curcumin assembly of complexing moieties, supported by ancillary ligands and collectively giving rise to soluble, bioavailable and biologically competent vanado-materials of distinct bioprofile.

To that end, the synthetic reactivity of the ternary system of V(IV) with curcumin and the ancillary aromatic chelator 2,2'-bipyridine (2,2'-bipy) was investigated in alcoholic media, ultimately leading to the isolation and physicochemical characterization of a crystalline ternary complex assembly. To the best of our knowledge, it is the third ternary system crystallographically characterized with the VO^{2+} moiety, curcumin as the ligand, and an incorporated N,N-aromatic chelator [**33**]. The structural composition and nature of the newly arisen material prompted further investigation of its biological reactivity profile, thereby setting the basis for its potential use as a hybrid metallopharmaceutical.

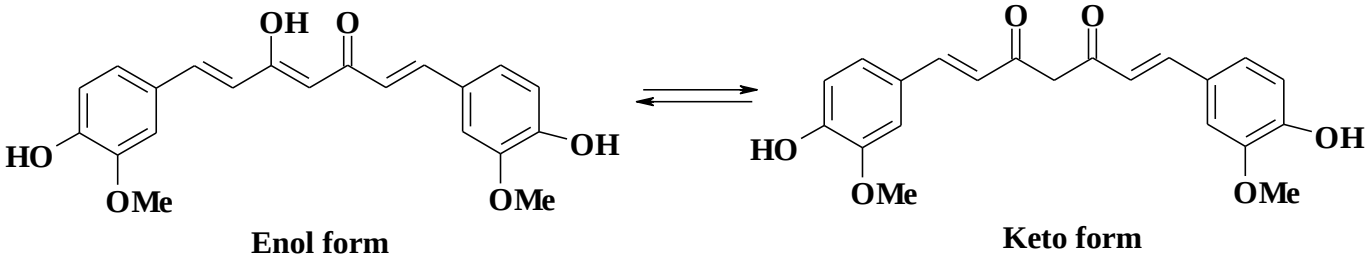

Scheme 1: Keto-enol tautomers of curcumin.

2. Experimental Section

2.1 Materials and Methods. All experiments were carried out under aerobic conditions. The structures of the employed ligands are shown in **Scheme 2**. The following starting materials were purchased from commercial sources (Sigma, Fluka) and were used without further purification: curcumin, 2,2'-bipyridine (2,2'-bipy), and vanadyl sulphate trihydrate ($VOSO_4 \cdot 3H_2O$). Solvents: methanol, diethylether. The isolated and dried under vacuum complex, at room temperature, is air-stable.

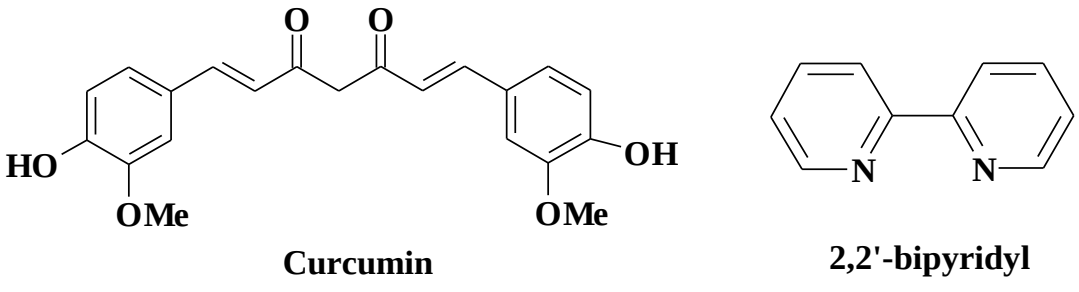

Scheme 2: Schematic representation of the ligands used in this study.

2.1.1 Physical measurements. FT-Infrared spectra were recorded on a Perkin Elmer 1760X FT-infrared spectrometer. A ThermoFinnigan Flash EA 1112 CHNS elemental analyzer was used for the simultaneous determination of carbon, hydrogen, and nitrogen (%). The analyzer operation is based on the dynamic flash combustion of the sample (at 1800 °C) followed by reduction, trapping, complete GC separation and detection of the products. The instrument is a) fully automated and controlled by PC via the Eager 300 dedicated software, and b) capable of handling solid, liquid or gaseous substances.

2.1.2 ESI-MS measurements. The Electrospray Spray Ionization mass spectrum was obtained on an Agilent Technology LC/MSD trap SL instrument and Thermo Scientific, LTQ Orbitrap XL™ high resolution system.

2.1.3 Solution NMR Spectroscopy. Solution ^{1}H- and ^{13}C-NMR experiments for **1** were carried out on Varian 600 MHz spectrometer. The sample concentration was ~5 mM. Freshly prepared material was dissolved in deuterated dimethyl sulfoxide (DMSO-d_6). The spectra were run 2h after complete dissolution of the sample. Carbon spectra were acquired with 5000 transients, a spectral width of 37000 Hz and a relaxation delay of 2 s. Proton spectra were acquired with 128 transients and a spectral width of 9000 Hz. Experimental data were processed using VNMR routines. Spectra were zerofilled and subjected to exponential apodization prior to FT. Chemical shifts (δ) are reported in ppm, while the spectra were referenced through the standard experimental setup.

2.1.4 UV-Visible measurements. UV-Visible (UV-Vis) measurements were carried out on a Hitachi U-2001 spectrophotometer, in the range from 190 to 1000 nm.

2.1.5 Fluorescence measurements. Steady state fluorescence emission and excitation spectra were recorded on a Hitachi F-7000 fluorescence spectrophotometer from Hitachi High-Technologies Corporation. The employed slit widths (em, ex) were 5.0 nm and the scan speed was 60 nm·min^{-1}. All measurements were carried out at room temperature. The entire system was supported by the appropriate computer software, FL Solutions 2.1, running on Windows XP.

2.1.6 Thermal studies. A Perkin Elmer, Pyris 1, system was used to run the simultaneous Thermogravimetric Analysis (TGA) experiments. The instrument mass precision is 1 μg. About 10 mg of compound **1** was placed in an open alumina sample pan for each experiment. High purity air was used at a constant flow rate of 30 mL·min^{-1}, depending on the conditions required for running the experiments. During the experiments, the sample weight loss and rate of weight loss were recorded continuously under dynamic conditions, as a function of time or temperature, in the range 30–850 °C. Prior to activating the heating routine program, the entire system was purged with the appropriate gas for 10 min, at a rate of 30 mL·min^{-1}, to ensure that the desired environment had been established.

2.1.7 Magnetization measurements. Magnetization measurements on a 20.2 mg powder sample of **1**were performed on a Quantum Design Vibrating Sample Magnetometer QD-Versalab in the 50–300 K temperature range and fields up to 3 T. Measurements were corrected for the diamagnetic contribution of the sample holder and Teflon wrap, -3.1x10^{-10} emu·Oe^{-1}, and the magnetic contribution of the brass half-tube sample

holder. The diamagnetic contribution of the compound ions was not taken into account as it is ~7.4×10^{-4} emu·mol^{-1} [**39**], five orders of magnitude lower than the experimental molar susceptibility, which is ~24 emu·mol^{-1} at room temperature in a field of 10000 Oe.

2.1.8 EPR measurements. Continuous wave (cw)X-band Electron Paramagnetic Resonance (EPR) measurements were performed on a Bruker ER 200D instrument, equipped with ESR-9Oxford cryostat and an Anritsu microwave frequency counter. Pulse EPR measurements at X-band (mw frequency 9.710 GHz) were performed on a Bruker ESP 380E spectrometer, equipped with an EN 4118X-MD4 Bruker resonator. Measurements at cryogenic temperatures were performed using a helium cryostat from Oxford Inc. The microwave frequency was measured using a HP 5350B microwave frequency counter and the temperature was stabilized using an Oxford ITC4 temperature controller. Hyperfine Sublevel Correlation (HYSCORE) spectroscopy with the pulse sequence $\pi/2$-τ-$\pi/2$-t_1-π-t_2-$\pi/2$-τ-echo was carried out with the following instrumental parameters: $t_{\pi/2}$ = 16 ns; starting values of the two variable times t_1 and t_2, 56 ns; time increment, Δt = 24 ns (data matrix 180 × 180). In order to eliminate blind-spot artifacts, up to three spectra were recorded with τ = 120, 144, and 168 ns. A four-step phase cycle was used to remove undesired echoes. The data were processed with the program MATLAB (The MathWorks, Natick, MA). The HYSCORE time traces were baseline corrected with a second-order exponential, apodized with a Gaussian window, and zero filled. After a two-dimensional Fourier transform the absolute-value spectra were calculated. The experimental cw EPR and HYSCORE spectra were simulated using the EasySpin package [**40**].

2.1.9 DFT calculations. The Vienna Ab Initio Simulation Package (VASP), version 5.3.3 [**41**], was employed in order to study the electronic structure of the title complex using Density Functional Theory (DFT). The Perdew-Burke-Ernzerhof (PBE) gradient-corrected exchange-correlation functional [**42**] was used along with the Grimme DFT-D2 method [**43**], in which van der Waals interactions are described via a pair-wise force field. All calculations were performed using plane-wave basis sets, and the Projector Augmented Wave (PAW) method [**44,45a**], with a plane-wave cut-off energy of 400 eV. In addition, a Γ centered k-point grid of 1×2×2 was employed for all calculations related to electronic structure, while geometry optimization involved a k-point grid of 1×1×1with maximum residual atomic forces of 0.01 eV·Å^{-1}. Gaussian smearing with a width of 0.05 eV was used to determine how partial occupancies are set for each wave function. The vanadium-curcumin complex was modeled using a simple monoclinic unit cell (**Fig. S1**) of dimensions a = 30.12 Å, b = 15.55 Å, c =15.94 Å, $\alpha = \gamma = 90°$, and β=116.18°, with a unit-cell volume of 6697.04 Å^3; initial crystal structure and atomic coordinates were taken from the crystallographic data described in section 3.2. The Nudged Elastic Band (NEB) method was used to extract the interconversion activation barrier between the cis- and trans-conformers in gas phase (**Fig. S1**). Seven intermediate configurations between cis- and trans- were created using an image dependent pair potential [**45b**], in which the maximum distance was set equal to 3 Å. Illustrations of the computational structures in this work were constructed using the visualization tool VESTA [**46**].

2.2 Synthesis

2.2.1 Preparation of $[VO(C_{21}H_{19}O_6)(C_{10}H_8N_2)(H_2O)]_2(SO_4)\cdot 2CH_3OH\cdot 3H_2O$ (1). To a solution of $VOSO_4\cdot 3H_2O$ (0.22 g, 1.0 mmol) in 10 mL MeOH, curcumin (0.37 g, 1.0 mmol) was added under stirring. The resulting brown solution was refluxed for two hours under continuous stirring and then cooled to room temperature. Subsequently, a solution of 2,2'-bipyridine (0.16 g, 1.0 mmol) in MeOH (5 mL) was added under continuous stirring. The resulting clear, dark red reaction mixture was refluxed for an additional 2 h and then cooled to room temperature. Subsequently, the reaction flask was placed at 4 ^oC and diethyl ether was added. Two weeks later, a crimson-colored crystalline material precipitated at the bottom of the flask. The product was isolated by filtration and dried in vacuo. Yield: 0.60 g (83%). Anal. Calcd for **1**, **$[VO(C_{21}H_{19}O_6)(C_{10}H_8N_2)(H_2O)]_2(SO_4)\cdot 2CH_3OH\cdot 3H_2O$ (1)**. ($C_{64}H_{72}N_4O_{25}SV_2$, M_r1431.23): C, 53.71; H, 5.07; N 3.91; S 2.24. Found: C, 53.68; H, 5.03; N 3.84; S 2.22.

2.3 X-ray crystal structure determination. X-ray quality crystals of **1** were grown from a mixture of methanol-diethyl ether. Crystals were taken from the mother liquor and mounted at room temperature on a Bruker Kappa APEX 2 diffractometer, equipped with a triumph monochromator, using Mo Kα radiation. Cell dimensions and crystal system determination were performed using 118 high θ reflections with $I>10\sigma[I]$. Data collection (φ- and ω-scans) and processing (cell refinement, data reduction and numerical absorption correction based on dimensions) were performed using the SAINT and SADABS programs [**47,48**]. The structure was solved through the SUPERFLIP package [**49**]. The CRYSTALS version 14.43 program package was used for structure refinement by full-matrix least-squares methods on F^2 and all subsequently remaining calculations [**50**]. Molecular illustrations were drawn with the Diamond 3.1 crystallographic package [**51**]. All non-hydrogen atoms have been anisotropically refined. All hydrogen atoms were found at their expected positions and were refined using proper riding constraints to the pivot atoms. Crystallographic details for **1**are summarized in **Table 1**. Further details on the crystallographic studies as well as atomic displacement parameters are given as Supporting Information and in the form of cif files.

2.4 Biological studies

Cytotoxicity is an important effect of new compounds, which must be taken into consideration when investigating living cells or tissues. It reflects the extent to which a chemical substance can damage an organism or a cell. By extension, the term may be metaphorically used to describe toxic effects on various organelles, such as mitochondria, the nucleus, membranes, etc. A comparative measure of compound effectiveness in inhibiting a specific biological or biochemical function is the half maximal inhibitory concentration (IC_{50}). To this end, cytotoxicity of the newly synthesized compound **1** was investigated against one of the most intensively studied eukaryotic model organisms, i.e. the fungal *Saccharomyces cerevisiae (S. cerevisiae)*, by two methods: monitoring a) growth by turbidity, and b) viability by fluorimetry.

2.4.1 Toxicity studies of curcumin and compound 1 against fungal yeast cells. The lyophilized yeast cells were suspended in solution (0.2 $mg\cdot mL^{-1}$) in MMS medium (1.5% (w/v) glucose, 0.5% (w/v) NH_4Cl, 0.5% (w/v) K_2HPO_4, 0.1% (w/v) NaCl, 0.01% (w/v) $MgSO_4\cdot 7H_2O$, and 0.1% (w/v) yeast extract; the pH of

the medium was adjusted to 7.0) and were grown for 16 h in an incubator, at 30 ºC under 200 rpm constant shaking. The growth of the culture was monitored by measuring turbidity/absorbance at 600 nm on a Selecta UV-2005 UV-Vis spectrophotometer. To that end, cells were diluted with fresh MMS to obtain cultures of ~0.4 turbidity. The cells were then allowed to grow for 24 h at 30 ºC under 200 rpm constant shaking, following exposure to curcumin, VO^{2+}, 2,2'-bipy and the title compound **1**, at several concentrations (2.5, 5, 10, 15, 20, 25, 40, 50 $\mu mol \cdot L^{-1}$). Dimethyl sulfoxide (DMSO) was used to dissolve-dilute both curcumin and **1**, with its final concentration in the cultures maintained below 2% v/v. Appropriate controls run on cultures containing a final concentration of 2% DMSO did not show any appreciable toxicity. Turbidity of the cultures was measured and graphed, as a function of substance concentration, to evaluate their effect on cell growth and determine the IC_{50} value. Control cultures (in the presence of the respective DMSO concentration alone) were run to monitor the effect of DMSO on cell growth. Cells from the respective cultures were harvested under centrifugation at 4,000 rpm for 5 min and then frozen, along with the extracellular media, for further analysis at -20ºC.

2.4.2 Determination of fungus viability. In view of the fact that determination of toxicity through turbidity measurements may not be fully reliable for toxicity assessment, determination of cell viability was also carried out. The principle of the fluorescein diacetate (FDA) method in cell viability determination is based on a measurable difference between fluorescein released by live cells compared to that released by dead or static cells due to toxicity, taking into consideration the fact that only live cells are able to hydrolyze FDA to fluorescein. Yeast viability, in the absence and presence of various concentrations of curcumin and the title compound, was evaluated through determination of the degree of hydrolysis of FDA to fluorescein by *S. cerevisiae* culture cells. FDA is hydrolyzed to fluorescein and acetic acid by different enzymes of the primary metabolism of fungi and micro-organisms, encompassing proteases, lipases, and esterases [**52**]. A stock solution of FDA in acetone (2 $mg \cdot mL^{-1}$) was added to reach a final concentration of 10 $\mu g \cdot mL^{-1}$ and the cultures were incubated at 37 ºC on a rotary shaker (120 rpm) for a total of 1 h. The reaction was terminated by diluting the reaction mixture with one volume of acetone and the released fluorescein was measured on an F-7000 FL Spectrophotometer (excitation: 494.0 nm; emission: 500-560 nm).

2.4.3 Lipid peroxidation by malondialdehyde determination. Quantification of lipid peroxidation is essential to assessing oxidative stress induced in various abnormal pathophysiological cellular situations, e.g. exposure to various chemical agents. One of the lipid peroxidation natural by-products forming is malondialdehyde (MDA), which is an endogenous genotoxic end-product of enzymatic and oxygen radical-induced lipid peroxidation. The MDA in the sample reacts with Thiobarbituric Acid (TBA) to generate the MDA-TBA adduct. The MDA-TBA adduct can be easily quantified colorimetrically (λ = 532 nm). Increase of MDA levels suggests higher lipid peroxidation [**53**]. Cell cultures alone and exposed to various concentrations of either curcumin or **1** were collected and boiled for 15 min in a buffer containing 100 mM NaCl, 1% (w/v) SDS, 2% (v/v) Triton X-100, 10 mM Tris-HCl pH 8.00, and 1 mM EDTA. Then, the samples were lysed by ultrasound (15 s, 10 cycles). Lysates were subsequently clarified by centrifugation (10,000

rpm for 15 min). A volume of 500 μL of either lysates or culture growth medium were a) dissolved in a solution containing 20% (w/v) trichloroacetic acid (TCA) and 0.67% (w/v) thiobarbituric acid (TBA), and b) boiled for 1 h. After cooling to room temperature, the reaction mixtures were centrifuged and the absorbance of the supernatant was measured at 532 nm to quantify the purple MDA-TBA product [**54**].

2.4.4 Oxidative stress by determination of Reactive Oxygen Species.

The term Reactive Oxygen Species (ROS) pertains to all reactive molecules and free radicals originating from molecular oxygen. The electronic structure of oxygen renders the molecule susceptible to radical formation. The generation of oxygen-based radicals, derived during the mitochondrial electron transport of aerobic respiration or redox enzymes and metal-catalyzed oxidation, leads to detrimental consequences. Sequential reduction of oxygen through addition of electrons leads to the formation of many ROS species, including superoxide ion, hydrogen peroxide, hydroxyl radical, hydroxyl ion, and nitric oxide. It is also noted that ROS can serve as both intra- and inter-cellular messengers. ROS generated intracellularly by *S. cerevisiae*, as a response to the exposure to various concentrations of curcumin and the title vanadium compound, were measured via the nitrobluetetrazolium chloride (NBT) reduction [**54**]. Fungal cells, collected from each of the previously mentioned cultures, were dispersed in 100 μL of MMS growth medium, and 500 μL of 1 $mg \cdot mL^{-1}$NBT solution was added. The reactions were run at 37 ^{o}C under shaking for 1 h and terminated with 100 μL of 0.1 N HCl. The mixtures were centrifuged at 1500 g for 10 min and the resulting pellets were dispersed in 600 μL of DMSO to dissolve the formazan product. Subsequently, 500 μL of MMS was added, the mixtures were centrifuged once again, and the absorbance of the supernatant derived from cell lysis was measured (intracellular ROS) at 575 nm, whereas the blue color of the supernatant (extracellular ROS) was measured at the same wavelength.

2.4.5 *In vitro* interaction experiments of curcumin and 1on eukaryotic or bacterial DNA. DNA interactions (cleavage/binding reactivity) with the title compounds was monitored following incubation of the latter with dsCTDNA or plasmid pUC18, followed by separation of the derived products using agarose gel electrophoresis. Specifically, the pDNA cleavage efficiency of these compounds was measured by determining their ability to convert the supercoiled (SC) or relaxed form (R) of pDNA to the nicked circular (NC) or/and linear form. Plasmid DNA preparation appears in two conformations: the supercoiled and open-circular forms. Given the presence of a break in only one of the strands in the latter species, DNA will remain circular, however, the strand break permits rotation around the phosphodiester backbone thus releasing the supercoils. Consequently, for the same DNA, the supercoiled conformation runs faster than the open-circular form. If DNA sustains double strand breaks, it produces a linear conformation. Linear DNA runs through a gel end first and thus involves less friction than open-circular DNA, yet more than supercoiled DNA, thereby migrating at a rate intermediate between the two.

For DNA damage experiments, native DNA (double-stranded DNA) (CT-dsDNA) type I, highly polymerized, from calf thymus glands, was purchased from Sigma (D-1501). Plasmid DNA, (pDNA) (pUC18) was isolated from *Escherichia coli* (Top 10) using the GenEluteTM HP endotoxin-free plasmid maxiprep prepa-

ration (Sigma–Aldrich), according to manufacturer specifications. The DNA stock solution (1 $mg \cdot mL^{-1}$) was prepared at 0–4 ^oC by dissolving the commercially purchased calf thymus DNA in buffer A (50 mMTris ((hydroxymethyl)amino methane)–HCl buffer (pH 7.5)). Agarose and the intercalating dye ethidium bromide (EtBr) were purchased from Invitrogen and Sigma, respectively.

Calf thymus double-stranded DNA (CT-dsDNA) was exposed to several concentrations of curcumin or **1**, at a constant temperature of 37 ^oC for 1 h, in buffer A, to a final volume of 20 μL, and the interaction products were separated using agarose gel electrophoresis. Reactions, containing aliquots of 3 μg of nucleic acid (dsCT-DNA) and various concentrations of curcumin or **1** after incubation, were terminated by adding 5 μL loading buffer, consisting of 0.25% w/v bromophenol blue and 30% v/v glycerol in water. The products resulting from interactions of curcumin and **1** with DNA were separated by electrophoresis on agarose gels (1% w/v), containing 1 $\mu g \cdot mL^{-1}$ EtBr in $40 \cdot 10^{-3}$ M Tris–acetate, pH 7.5, $2 \cdot 10^{-2}$ M sodium acetate, $2 \cdot 10^{-3}$ M Na_2EDTA, at 5 $V \cdot cm^{-1}$. Agarose gel electrophoresis was run in a horizontal gel apparatus (Mini-SubTM DNA Cell, BioRad) for about 4 h. The gels were visualized under a UV illuminator, following staining with the fluorescence dye ethidium bromide due to its intercalation into the double stranded DNA.

2.4.6 Statistical analyses. Origin Pro 9.0 (Origin Lab Corporation) was employed for the statistical analysis and graph construction. Results are presented as means (SEMs), with standard deviation (SD) depicted as error bars and the experiments having been run as triplicates. One-way analysis of variance (ANOVA) test was used for discriminating between groups tested. For statistical significance to be reached (ns, $p>0.05$), a value of $p<0.05$ (*) was pre-requisite, with $p<0.1$ (**) and $p<0.001$ (***).

3. Results

3.1 Synthesis. The synthetic exploration of the ternary V(IV)-curcumin-(2,2'-bipy) system in this work followed carefully designed approaches. To that end, the **$[VO(C_{21}H_{19}O_6)(C_{10}H_8N_2)(H_2O)]_2(SO_4) \cdot 2CH_3OH \cdot 3H_2O$ (1)** material was synthesized in a facile fashion from simple reagents in alcoholic solution. In a typical reaction, $VOSO_4 \cdot 3H_2O$ reacted with curcumin using methanol as a solvent. The overall stoichiometric reaction leading to **1** is shown schematically below:

$$2VOSO_4 \cdot 3H_2O + 2C_{21}H_{20}O_6 + 2C_{10}H_8N_2 + 2\,CH_3OH \longrightarrow$$

$$[VO(C_{21}H_{19}O_6)(C_{10}H_8N_2)(H_2O)]_2(SO_4) \cdot 2CH_3OH \cdot 3H_2O + H_2SO_4 + H_2O$$

Diethyl ether was added as a precipitating solvent to the reaction mixture. A crimson-colored crystalline material emerged in the reaction described above, the analytical composition of which was consistent with the formulation in **1** (*vide supra*). Positive identification of the crystalline product was achieved by elemental analysis, FT-IR spectroscopy and X-ray crystallographic determination for isolated single crystals from **1** (*vide infra*). The complex is stable in the crystalline form, in the air, for fairly long periods of time. It is readily dissolved in methanol, DMSO, and DMF, moderately soluble in water and ethanol, and insoluble in acetone, acetonitrile, and dichloromethane at room temperature.

The scarcity of crystallographically characterized metal complexes of curcumin is also proved by relevant literature surveys that yielded ca. 150 publications in which only 13 crystal structures of such complexes are reported [**55**]. A summary of previous scientific works on the synthetic procedures of the crystallographically characterized curcumin complexes is presented in **Table 2**.

Table 2: Summary of synthetic procedures of crystallographically characterized curcumin complexes.

Starting metal salt	**Chelator**	**Added cation**	**Solvent**	**Metal salt to ligand molar ratio**	**Metal salt to chelator molar ratio**	**Metal salt to added cation molar ratio**	**Precipitation-crystallization method**	**Reference**
$VO(ClO_4)_3$	1,10-phenanthroline	Et_3N	CH_3CN/EtOH	1:1	1:1	1:1	Slow evaporation of the complex in acetonitrile at room temperature	**33,56**
$VO(ClO_4)_3$	dipicolylamine	Et_3N	CH_3CN/EtOH	1:1	1:1	1:1	Vapor diffusion of diethyl ether into solution of the complex in acetonitrile	**57**
$Zn(O_2CCH_3)_2(H_2O)_2$	-	-	DMA/EtOH	1:1.8	-	-	Heating in a closed vessel at 75 °C	**58**
$C_6H_5B(OH)_2$	-	-	CH_2Cl_2	1:1.17	-	-	Slow evaporation of the complex in CH_2Cl_2 in the fridge	**59**
$ZnCl_2$	dinonyl-2,2′-bipyridine	Et_3N	CH_2Cl_2	1:1	1:1	1:1	Slow evaporation at room temperature	**60**
$ZnCl_2$	4,4′-bis(hydroxymethyl)-2,2′-bipiridine	Et_3N	Acetone	1:1	1:1	1:1	Slow evaporation at room temperature	**60**
$La(NO_3)_3{\cdot}6H_2O$	4′-phenyl-2,2′:6′,2″-terpyridine	Et_3N	MeOH	1:1	1:1	Until pH 7.5	Slow evaporation of a solution of the complex in a MeOH–MeCN mixture	**61**
$Gd(NO_3)_3{\cdot}6H_2O$	4′-phenyl-2,2′:6′,2″-terpyridine	Et_3N	MeOH	1:1	1:1	Until pH 7.5	Slow evaporation of a solution of the complex in a MeOH–MeCN mixture	**61**
$[(p\text{-cymene})RuCl_2]_2$	-	NaOMe	MeOH	½:1	-	½:1	Recrystallization in $CHCl_3$ and slow evaporation at 4 °C	**62**
$[(\eta^6\text{-p-Cymol})RuC1_2]_2$	-	NaOH	MeOH	1:1	-	1:1.5	Slow evaporation of a methanol, or ethanol, or $CHCl_3$/Pentane solution	**63**
fac-$[Re(CO)_3(H_2O)(acac)]$	triphenylphosphine	-	MeOH	1:1	1:2	-	Slow evaporation of a toluene/ ethanol/methanol solution	**64**
$[Ru(cymene)Cl_2]_2$	1,3,5-triaza-7-phosphaadamantane	KOH	MeOH	0.5:1	0.5:1	0.5:1	Recrystallization from a mixture of dichloromethane and n-hexane and slow evaporation at 4 °C	**65**
$[Ru(hmb)Cl_2]_2$	1,3,5-triaza-7-phosphaadamantane	KOH	MeOH	0.5:1	0.5:1	0.5:1	Recrystallization from a mixture of dichloromethane and n-hexane and slow evaporation at 4 °C	**65**

3.2 Description of X-ray Crystallographic Structure

The X-ray crystal structure of **1** reveals a discrete solid state lattice. The structure of the vanadium assembly in **1** is shown in **Fig.1**. Selected bond distances and angles are listed in **Table 3**. Compound **1** crystallizes in the monoclinic space group C2/c. The asymmetric unit contains one singly cationicV(IV) complex assembly, a one half sulfate dianion, one and half lattice water molecules and one lattice methanol molecule. The structure of **1** shows an oxidovanadium(IV) moiety, bound to the chelating *N,N*-donor 2,2'-bipy, *O,O*-donor singly anionic curcumin and one water molecule, thus giving rise to a $V^{IV}N_2O_4$ coordination sphere in a distorted octahedral geometry. The V-N and V-O (curcumin) distances are in the range of 2.081(2) to 2.128(2) Å, and 1.956(2) to 1.964(2) Å, respectively. The equatorial plane, arising from the coordinated atoms, originates in the *N,N*-donor and *O,O*-donor ligands, with the axial positions being occupied by the oxidovanadium(IV) oxygen atom and the coordinated water molecule. The V=O bond distance is 1.587(2) Å. The V-O bond trans to the V=O group is long (2.308(2) Å), indicatingthattheV-OH_2 bond could readily dissociate in solution as also suggested by ESI-MS (vide infra).The V-N and V=O distances were found to be consistent with those reported in the literature [**33,66**]**.** Seven hydrogen bonding interactions were found (**Table S1**) to contribute to a three dimensional (3D) crystal lattice. Of the curcumin phenolic hydrogen atoms, the first one interacts with the oxygen atom from a neighboring oxidovanadium(IV) moiety and the second one with an oxygen atom from the sulfate anion. All four oxygen atoms from the sulfuric acid anion as well as the lattice water molecules bridge the lattice methanol molecule and the coordinated water ligand, thus forming a strong hydrogen-bonding network. The lattice can best be described as one assembled through parallel complex equatorial plane moieties in layers, connected with hydrogen-bonding interactions through the coordinated water, oxidovanadium and sulfate anion oxygen atoms.

3.3 FT-IR spectroscopy. The FT-IR spectrum of **1** shows three bands at 1596 cm^{-1}, 1508 cm^{-1} and 993 cm^{-1}, which can be attributed to the C=O, C=C (β-diketonate) and V=O stretching vibrations. The bands appearing in the 667-768 cm^{-1} range and at 1030 $cm^{-1}$are attributed to the V-O stretching mode [**67**]. The band at 470 cm^{-1} corresponds to the V-N bond [**68**]. The frequencies of the observed vibrations were shifted to lower values, in comparison to the corresponding vibrations in free curcumin, thus indicating changes in the vibrational status of curcumin upon binding to the V(IV) ion. All observations were further attested to by the X-ray crystal structure of **1**.

3.4 ESI-MS studies. The high resolution ESI-MS of **1** in H_2O showed a peak corresponding to the $[M\text{-}H_2O]^+$ (**Fig. 2**). The mass spectral data and the associated simulations suggest the presence of the complex species $[VO(C_{21}H_{19}O_6)(C_{10}H_8N_2)]^+$.

3.5 Solution NMR spectroscopy. The room temperature ^{1}H-NMRand ^{13}C-NMR spectra of **1**in DMSO-d_6 (**Fig. 3A-3B**) showed characteristic spectral features of the metal-bound bipyridine ligand and the β-diketonato moiety. The signals in the ^{1}H-NMR spectrum are in agreement with a 1:1:1 metal:(N,N-ligand):curcumin stoichiometry [**69**]. The spectra are not identical with those of free bipy and curcumin in the same solvent and under identical experimental conditions, indicating a) the significant influence of the paramagnetic center on the ligands upon coordination, and b) formulation of the identity of **1** in solution

[**69,70**]. The signals from the aromatic protons (h, i) and (b) as well as the olefinic proton (f) coalesce in the ^{1}H-NMR spectrum of **1**, as do the signals from the aromatic proton (j) and the olefinic proton (g). Moreover, the phenolic proton (k) exhibited a broad feature in comparison to literature reported ^{1}H-NMR spectra of free curcumin [**71-73**]. No significant shifts were observed for the protons compared to free curcumin and 2,2'-bipy, respectively. The spectrum in (**A**) indicatively shows the peak (marked as **e**) at ~5.9 ppm, corresponding to the C-H proton of the β-diketone moiety. Its relatively low intensity is due to the prolonged retention of the compound in solution [**33**]. In the case of the ^{13}C-NMR spectrum of **1**, no signal was observed for the two carbonyl carbons (C-6) and no significant shifts were observed for all carbons in comparison to free curcumin and 2,2'-bipy. However, the intensity of the signals was significantly reduced compared to that of unbound curcumin and 2,2'-bipy [**61-63**].

3.6 UV-Vis spectroscopy. The UV–Vis spectra of pure curcumin and **1** were recorded in methanol at a concentration of 10^{-6} M (**Fig. 4A**). Free curcumin exhibits an absorption maximum at 430 nm and a weak absorption band at 278 nm. The maximum absorption is assigned to the π–π* transitions in the enolic form in solution [**74,75**]. A shift in the observed absorption maximum [**76-80**], is linked to the ionization of the phenolic OH group, leading to a bright red-colored phenoxide moiety [**75,81-83**]. In view of the aforementioned curcumin features, the electronic spectrum of **1** exhibits a similar pattern with the spectrum of curcumin, involving an intense absorption maximum at 446 nm (λ_{max}, ε~138,000 $M^{-1}\cdot cm^{-1}$), and an absorption band at 279 nm (ε~109,000 $M^{-1}\cdot cm^{-1}$). The observed bathochromic shift in the intense absorption for **1**, compared to free curcumin, is indicative of its extended conjugation and coordination to the metal center [**84-88**]. **Fig. 4B** presents the electronic d-d transitions of **1** at lower energies and at concentrations higher than 10^{-6} M. The d-d band appears as a shoulder at around 300 nm upon increase in the concentration of **1**.

3.7 Fluorescence studies. Steady state fluorescence measurements of emission and excitation spectra of pure curcumin and **1** were recorded in methanol, at a concentration of 10^{-6} M and at room temperature (**Fig. 5**). The results at hand suggest that free curcumin exhibits an emission with a single broad band around 537 nm, when excited at 372 nm, which could be attributed to aromatic π−π* transitions. The broadening of the spectrum is assigned to the methanol interactions with the enolic protons of the keto-enol moiety [**89**]. The emission spectrum of **1** shows a quenched single broad band with an emission maximum at 539 nm, when excited at 405 nm, which could be attributed to aromatic π−π* transitions. The observed quenching, compared to the free ligand, could be attributed to the ligand coordination effect reflected into the presence of the deprotonated curcuminato ligand bound to V(IV). This fact is common in paramagnetic metal centers that normally act as quenchers, displaying chelation enhancement of quenching (CHEQ) effects [**90,91**].

3.8 Thermal studies. The thermal decomposition of **1** was studied by TGA under an atmosphere of air (**Fig. 6**). Compound **1** is thermally stable up to 44 °C. From that point on, a fairly broad heat process points to the dehydration and solvent removalof **1**, with the release of moisture and lattice water and methanol molecules between 44 ºC and 232 ºC. In fact, a 9.3% drop in weight, from the start of the thermal treatment until 108 ºC, is consistent with the release of the two methanol and three water molecules in the lattice, along

with the sole water molecule in the coordination sphere of vanadium, consistent with the theoretically expected value of 9.5%. Between 232 ºC and 454 ºC, further weight loss is observed, in line with the decomposition of the organic structure of the molecule. No clear plateaus are reached in this temperature range, suggesting that the arising products are unstable and decompose further. A plateau in the decomposition of **1** is reached at 454 °C, with no further loss up to 700 °C, in line with the thesis that the product at that temperature and beyond (700 °C) is V_2O_5. The violent reaction observed at around 728 ºC, not associated with mass loss,may be related to a crystalline structural change [**92**], or the melting of the product of the thermal decomposition reaction, V_2O_5. The total weight loss of ~87.4% is in agreement with the theoretical value ~87.4%, according to the following equation:

$$\mathbf{[VO(C_{21}H_{19}O_6)(C_{10}H_8N_2)(H_2O)]_2(SO_4)\cdot 2(CH_3OH)\cdot 3H_2O \; + \; 77O_2 \longrightarrow}$$

$$\mathbf{V_2O_5 \; + \; 64CO_2 \; + \; SO_2 \; + \; 4NO_2 \; + \; 36H_2O}$$

Examination of the residue by Scanning Electron Microscopy (SEM) (**Fig. S2**) and powder XRD showed the presence of oxides, ordinarily obtained under oxidative conditions, and consistent with previously reported results of TGA on vanadium-containing species [**93,94**].

3.9 Magnetization measurements. The temperature dependence of the effective magnetic moment μ_{eff} and μ_{eff}*T of **1** in a field of $\mu_0 H$ = 1 T (10000 Oe) is shown in **Fig. 7**. Magnetic susceptibility is paramagnetic, inversely proportional to temperature. Fitting the molar magnetic susceptibility to the Curie law,

$$\chi_{mol} = C_{mol}/T$$

the molar Curie constant C_{mol} = 0.686 $cm^3 \cdot K \cdot mol^{-1}$ (8.62 x 10^{-6} $m^3 \cdot K \cdot mol^{-1}$) is obtained.

The paramagnetic effective magnetic moment μ_{eff} is deduced from

$$C_{mol} = N_{AV} g^2 \beta^2 S(S+1)/3k_B$$

where β is the Bohr magneton, N is Avogadro's number, g is the Landé factor, and k_B is the Boltzmann constant. Taking into account that there are two vanadium atoms per formula unit, the experimental effective magnetic moment is 1.69 μ_B. The theoretical effective moment is μ_{eff}=1.55 μ_B, in line with the equation

$$\mu_{eff} = g[J(J+1)]^{1/2}\mu_B$$

where J is the total angular momentum quantum number, and g the Landé factor, of an isolated V(IV) $[Ar]3d^1$ ion,with a total spin quantum number S=1/2, and total angular momentum quantum number L=2 (J=L-S=3/2 and g=0.8). In oxidovanadium(IV) complexes, the crystal field of surrounding ions quenches the angular momentum (L=0, J=S and g=2) [**95-97**], so that the theoretical spin-only magnetic moment is μ_{eff}= 1.73 μ_B, with V(V) $[Ar]3d^0$ exhibiting a zero spin moment. The experimental magnetic moment of vanadium in **1** is quite close to the theoretical spin-only value of V(IV), μ_{eff} =1.73 μ_B, indicating that the oxidation state is 4+ [**98**].

3.10 EPR studies. The CW-EPR spectrum of **1** in a methanol/toluene (1:1) frozen solution, recorded at 70 K, is shown in **Fig. 8**. The spectrum is consistent with a mononuclear vanadyl species and can be simulated with the following spin Hamiltonian:

$$H = \beta S g B + I A^V S$$

where S = 1/2, the electronic spin, β is the Bohr magneton, B is the external magnetic field, I =7/2 is the nuclear spin of the ^{51}V nucleus, and A^V is the hyperfine interaction tensor. The experimental spectrum is reproduced with the following parameters:

g_x=1.979(1), g_y=1.978(4), g_z = 1.940(6), A^V_x = 178 MHz,A^V_y=191 MHz, A^V_z = 506 MHz.

Moreover, in order to a) reveal weak hyperfine couplings with ligand atoms participating in the coordination sphere of vanadium, and b) gain further insight into the electronic structure and coordination mode of the ligands in **1**, HYSCORE experiments were carried out at 40 K [**99**]. The relevant spectra are shown in **Fig.9A-C**. Specifically, the HYSCORE spectrum reveals several correlation peaks, both in the left and right quadrant. The cross-peaks at (-9,5) and (-5,9) MHz are separated by approximately four times the nuclear Zeeman frequency of ^{14}N, $4\nu_{14N}$ = 4 MHz. In that respect, they are assigned to a strongly-coupled nitrogen atom with a hyperfine coupling A ≈ 6.5 MHz. A successful simulation is obtained assuming two nitrogen atoms with identical principal axis system (PAS) parameters shown in **Table 4**. The isotropic hyperfine interaction (HFI) a_{iso} = -6.3 MHz and the nuclear quadrupole coupling constant $K = e^2qQ/4h$, with the asymmetry parameter $\eta = (Q_x–Q_y)/Q_z$, are typical for equatorially coordinated nitrogen atoms in $[V^{IV}O]^{2+}$ vanadyl complexes [**100**]. The simulation reproduces well both the shapes and relative intensities of most correlation peaks. However, the strong peaks in the right quadrant, marked by arrows in **Fig.9A**, cannot be obtained with these parameters, since they correspond to a weakly-coupled nitrogen atom with a hyperfine coupling $A<2\nu_{14N}$. **Fig.9C** shows the simulation using the previous parameters for the strongly-coupled nitrogen atom, but now a smaller coupling with a_{iso} = 0.9 MHz is assumed for the second nitrogen (**Table 5**). The latter hyperfine coupling is in line with axially coordinated nitrogen atoms in vanadyl complexes [**101**].

Comparing the experimental spectrum of **Fig. 9A** with the simulations of **Figs. 9B** and **9C**, it is clear that the parameters in "set 2" reproduce satisfactorily all correlation peaks. Therefore, based on the HYSCORE analysis, it is concluded that in solution, one of the 2,2'-bipynitrogen atoms occupies an axial position, relinquishing its place to equatorial coordination with a water or solvent molecule. This effect is well-known for vanadyl complexes and has been verified with ESEEM experiments in the past [**102**]. It is worth noting, however, that a mixture of both species (set 1 and set 2) cannot be excluded at this juncture, as the sum of their corresponding simulation spectra (**B** and **C** with an approximate 1:1 contribution) would still reproduce well all features of the experimental HYSCORE spectrum (vide infra).

3.11 DFT calculations. In order to look closely at the electronic structure of the vanadium-curcumin complex, DFT calculations were performed following the procedure described in section 2.1.9. The total density of states (DOS) as well as the projected density of states from individual contributions of V, O, C, N, S, and H atoms of the complex is shown in **Fig.10A**. The Fermi level (0 eV) is found to be located at ~0.2 eV above the conduction band minimum, which displays a major contribution from V3*d* orbitals and a small hybridization with O and C2*p* orbitals. To further investigate the origin of these states, their corresponding partial charge density was plottedin **Fig.10B**, showing that charge density being strongly localized on the V

atom, with moderate localization on the surrounding O, C, and N atoms. This provides evidence that the vanadium ion acts as the coordination center, while oxygen, carbon and nitrogen atoms constitute part of the surrounding ligand environment. In order to quantify this picture, net charge analysis [**103**] was performed to locate charge transfer occurring within the coordination assembly. It appears that, on average, there is a depletion of charge of ~1.00 |e| from the O7, ~0.84 |e from the O1 and O2, and ~0.75 |e| from the O31 atoms. In addition, charge depletion of ~1.12 |e| is observed from the N1 and N2 atoms. Finally, charge transfer of ~1.02 |e| is observed, on average, from the ligand toward the coordination center, i.e. the vanadium atoms, giving rise to the appearance of filled 3*d* vanadium states at the conduction band edge (**Fig.10A**), as experimentally attested to through UV-Vis spectroscopy (vide supra).

EPR measurements performed on the sample (Section 3.10) suggest two potential conformers present in solution, i.e. a trans- and a cis- (**Fig. S1B**) (vide supra). DFT calculations, using the Nudged Elastic Band method (Section 2.1.9), were performed to gain insight, in terms of a potential interconversion process, by extracting the energy activation barrier required for the conformational change from the trans- to cis- conformer and vice versa. As observed in **Fig. 11**, the total energy of the trans-conformer is 0.14 eV higher than the cis conformer, thus indicating that the latter species is most stable energetically. In addition, the activation barrier required for the interconversion from trans- to cis-conformer is found to be 0.25 eV, while the activation barrier for the opposite process, i.e. interconversion from cis- to trans-, is found to be 0.39 eV. This is an indication that conversion from trans- to cis-conformer is favorable, a finding consistent with the state of a rising (upon dissolution of **1**) equilibrium toward the cis conformer as suggested via EPR measurements (vide infra).

3.12 Toxicity of the compounds against fungal yeast cells. For the investigation of potential toxicity effects of both natural curcumin and the newly synthesized compound **1**, yeast cells were grown in the presence of various concentrations of each substance. Control cultures were also prepared in the absence of curcumin and **1**. Inhibition of cell growth and toxicity of these compounds was determined by measuring both culture turbidity and viability through metabolic enzymatic activity compared to control cultures. As can be seen in **Fig. 12**, growth of cultures is inhibited gradually in a concentration-dependent manner, in both cases. The observed inhibition reached ~15% in the presence of the highest concentration of curcumin (50 μM, $p<0.05$) compared to the control culture, but it was more pronounced in cultures grown in the presence of **1**, approaching 50% for the same concentration ($p<0.05$). The results afforded an IC_{50} value of >100 μM for curcumin, with the IC_{50} value of **1** being lower (53±3 μM), but still high. Fungal growth after treatment with solely 2% (v/v) DMSO did not inhibit growth significantly (10±4%, $p>0.05$). Control studies for pure $VOSO_4$ and 2,2´-bipy were also conducted (**Fig. S3**). No significant toxicity changes were noticed in the presence of either compound.

3.13 Fungal cell viability. Yeast cell viability fell to 50% compared to the control, in the presence of 10 μM curcumin, whereas for a similar effect, a concentration of 20 μMof **1**was required. Thus, the calculated IC_{50} value of fungal cell viability for **1** is equal to 20±2 μM in comparison to pure curcumin (10±1).It can be

concluded that a concentration of up to 10 μM of **1** could be considered non-toxic, as no more than a 10% drop in growth or viability was observed, whereas the same concentrations of pure curcumin seem to disturb the metabolic activity of the cells. Taking into consideration the fungal growth experiment, it came as a surprise, however, from the viability experiments, that the enzymatic potential of cells toward FDA-hydrolysis is lower (or defective) in curcumin-treated than in compound **1**-treated yeast cells, at almost all concentrations tested, a fact reflected in a pattern of two parallel curves (**Fig. 13A**). At concentrations higher than 25 μM, cell viability remained at 20% and 10% levels compared to control cultures in the presence of curcumin and **1**, respectively. It should also be noted that part of the inhibition observed at such high concentrations of both curcumin and **1** may be attributed to the presence of the employed DMSO in the cell cultures (data not shown). A representative figure (**Fig. 13B**) of cell viability shows the emission intensity curves of *S. cerevisiae* cells exposed to 5 μM and 25 μM of curcumin and **1**, compared to non-exposed cells, as a function of the excitation wavelengths. Obviously, the viability of *S. cerevisiae* cells exposed to 5 μM of **1** is higher than that of curcumin for the same concentration and in both cases lower than that of the non-exposed fungal cells.

3.14 Oxidative stress studies. Curcumin is a well-referenced anti-oxidant compound. Therefore, a main target of this study was to a) initially verify previous results on the anti-oxidant activity of curcumin-based compounds, and b) ultimately investigate the anti-oxidant potential of the newly-synthesized compound **1**. Two major markers of oxidative stress were studied: MDA – a product of lipid peroxidation, and ROS production.

3.14.1 Lipid peroxidation through MDA Determination

Lipid peroxidation was indirectly measured by monitoring MDA production in the presence of cell cultures, as a result of the exposure to curcumin and **1**. MDA levels compared to control (and control containing 2% DMSO) are presented for various concentrations of curcumin and **1**, as measured in cell lysates (intracellular MDA) and growth medium (extracellular MDA), respectively. Fungal cells exposed to either curcumin or **1**, in the concentration range 5-25 μM, caused reduction of intracellular MDA levels (up to ~25%) compared to control. This result may strongly support the notion that cells exposed to curcumin or **1** (at low concentrations up to 25 μM) amplifies cellular protection intracellularly against lipid peroxidation by lowering MDA levels ~15% compared to control cells. Interesting enough was the observation that MDA levels, produced by fungal cells intracellularly at the highest concentrations (40 and 50 μM), were higher in curcumin-exposed cells than in cells exposed to **1**. Specifically, in curcumin-exposed cells, MDA levels, at the respective concentrations, reached 160% and 207% of the control, respectively, thus revealing that **1** is able to significantly reduce (abolish) MDA levels generated by curcumin alone. In conjunction with that result, it is important that in the case of cells exposed to **1** at high concentrations (40 and 50 μM), MDA levels seem to be maintained close to control levels (**Fig. 14A**). On the contrary, extracellular MDA levels of fungal cells exposed to curcumin and **1** increased gradually in a concentration-dependent manner (from 10 to 50 μM),reaching a maximum value of 170% compared to control, whereas in fungal cells exposed to **1** extracel-

lular MDA levels remained at control levels until 10 μM, subsequently increasing at higher concentrations to 250%. Specifically, when fungal cells are exposed to concentrations higher than 15 μM, the extracellular MDA levels are higher in the case of **1** compared to curcumin for the same concentrations (**Fig. 14B**). In conclusion, to justify this result and taking into consideration the results obtained from the intracellular MDA levels, it appears that **1** seems to be a more potent chemo-protective agent against harmful MDA than curcumin under the experimental conditions and the model organism employed. The behavior indicates a cell protection mechanism, whereby various toxic agents are exported from the cell interior, as MDA levels were found to increase in the extracellular medium.

Experiments were also carried out for $VOSO_4$ and 2,2´-bipy. Interestingly, both of these compounds bear a significant, yet opposite effect, on both intracellular and extracellular levels of MDA. A 10 μM concentration of 2,2´-bipy raised extracellular MDA levels up to 119% compared to control, an effect that dwindled gradually, amounting to an 88% drop of MDA levels, when 50 μM of 2,2´-bipy was used. Increasing $VOSO_4$ concentration caused a commensurate drop of extracellular MDA levels, up to 73% at 50μM (**Fig. S4**). When intracellular MDA levers were assessed, however, there was a profound decrease of their levels when 2,2´-bipy concentration rose (up to 21% at 40 and 50 μM) and a profound increase when $VOSO_4$ levels rose (up to 333% at 25 μM) (**Fig.S5**). It is, thus, obvious that it is rather difficult to explain the effect of compound **1**on MDA levels, as MDA by-products may be gradually released as a result of the metabolic activity of the yeast cells and they induce different effects on the oxidative status of lipids.

3.14.2 ROS generation

ROS generated continuously during aerobic metabolism are highly reactive molecules. When in excess, they can lead to protein and DNA oxidation, protein cross-linking, and cell death. Oxidative stress-induced damage, resulting from excessive accumulation of ROS within cells and/or their release into the culture media, is highly cell type-specific, and there is a difference in the capacity of various cell types to produce and/or release ROS in response to the same stimulus. Although cells that produce and accumulate large amount of ROS within themselves can have detrimental effects on their own survival, the cells that are able to release a large amount of ROS extracellularly can cause damage to other cells. ROS are unstable and have a short life in the extracellular medium. In that respect, the antioxidant potential of curcumin and compound **1** was evaluated in terms of either intracellular ROS generation or scavenging by the fungal S. *cerevisiae* cells exposed to them. It is noteworthy that **1**, at low concentrations, attenuates oxidative stress intracellularly in fungal cells exposed to it, reflected in the decrease of $O_2^{-\bullet}$ in the fungal cytoplasm, reaching as low as 10%, with curcumin reaching 62%, compared to control (for 25 μM).This effect of **1**occurred by lowering the levels of intracellular ROS more drastically compared to those of the parent curcumin. Even minimal quantities of **1** (2.5 μM) could lower ROS levels to 22%, whereas the corresponding drop in the case of curcumin was 40%, compared to control. For all concentrations studied, compound **1** exhibited far better ROS-scavenging ability in comparison to curcumin. When fungal cells were treated with curcumin, lower ROS levels (42.5% compared to control) were observed at a concentration of 2.5 μM. ROS levels, as

a response to exposure of fungal cells to 10 μM and 50 μM curcumin alone, increased to 145%and 207%, respectively. In contrast to that, a 10 μM concentration of compound **1** lowered ROS to 30%. When the concentration of **1** was raised to50 μM, a reduction of the ROS levels compared to pure curcumin (207%) took place down to the control level (100%) (**Fig. 15**). Moreover, $VOSO_4$ and 2,2´-bipy are both inducers of oxidative stress, as they induced an increase of ROS levels up to 124% and 123%, respectively, at a concentration of 50 μM (**Fig. S6**).Thus, the anti-oxidant potential of **1** can be noted based on ROS-lowering activity reflecting measured ROS radical levels.

3.15 *In vitro* effect of curcumin and compound 1 on DNA. One of the most significant targets in the design and use of several anticancer drugs is DNA and the investigation of their interaction with it. There is plenty of biological and biochemical evidence on the existence of MDA contribution to DNA damage or MDA-induced DNA interstrand cross-links that a) could result from endogenous oxidative stress, and b) likely have biological effects on human cell physiology-pathology [**104**].

To probe potential DNA interactions (binding and/or damage) with **1**, treatment of CT-dsDNA was investigated at various concentrations of both curcumin and **1**. The treatment in both cases led to a concentration-dependent DNA degradation, as deduced by a) quantitation of the decrease (~65%) of the intensity of the main DNA band integrity for the highest concentration of curcumin tested (50 μM) (**Fig. 16A, lane 8**), and b) the extent of band smearing. The decrease was more pronounced at all concentrations tested in the presence of **1** (**Fig. 16A, lanes 1´-8´)** compared to control and curcumin alone (**Fig. 16A, lane 1-8**), and reached ~73% in the presence of 50 μM(**Fig. 16A, lane 8´**), reflecting reduction of intensity, until the disappearance of the main DNA band. The effects on DNA were summarized and plotted in **Fig. 16B**. As a comparison, it is noted that loss of 50% DNA integrity was caused by 15 μM of compound **1**, whereas the same result occurred at 25 μM of curcumin.

In addition, plasmid DNA (pDNA)(containing both supercoiled **S** and relaxed **R** forms) was treated with various concentrations of curcumin or **1** and the products were separated by agarose gel electrophoresis in mobility shift experiments. In both cases, an up-shift of pDNA was observed, exhibiting delayed electrophoretic mobility, due to compound binding, thus resulting in aggregated or multimeric DNA forms remaining in the wells and being unable to enter the gel. More interesting was the observation that incubation with **1** led to the degradation of the supercoiled DNA band (**S**) compared to control and curcumin alone (disappearance of the respective band) at low concentrations (**Fig. 16C, lanes 1´-4´**),whereas at higher concentrations, formation of a new band emerged that was barely visible. The latter species exhibited delayed electrophoretic mobility compared to both pDNA bands, likely reflecting the presence of pDNA dimer (**D**) or multimer (**M**) forms as a result of the title complex interaction(s) (**Fig. 16C, lanes 6´-7´**). Finally, attenuation of the intensity of all DNA bands occurred due to degradation (**Fig. 16C, lanes 7´**) compared to control. The observed differential behavior of interaction mode of both compounds with a) CT-dsDNA, causing gradual concentration-dependent degradation, and b) pDNA, causing aggregation rather than degradation, might be

attributed to the difference of the secondary and supercoiled structures of pDNA, being differentially accessible for facile intercalation as in CT-dsDNA, thereby pointing toward an intercalating mode of action.

4. Discussion

4.1 Synthetic challenges in ternary metal-curcumin systems

The bioactivity of physiological substrates of natural origin depends to a great extent on their a) structure, b) solubility and bioavailability, and c) chemical reactivity at the biochemical level. Among such well-known physiological organic substrates, currently under investigation, curcumin emerges as a primary target of pharmaceutical significance due to its biologically confirmed pharmacological value. Its poor solubility and bioavailability, however, stand as an impediment in further achieving higher levels of selective and specific biological effects toward disease therapeutics. Metal ions, on the other hand, have been known to exert beneficial action(s) at the cellular level through appropriate configuration of their coordination sphere, thereby formulating key interactions with molecular targets linked to the (patho)physiology of cells. Vanadium is one of those transition metal ions, for which a diverse spectrum of reactivities have shown it to be useful in treatments of various diseases, including diabetes, cancer, and others. In view of that metal ion's flexibility to commit to (bio)chemical reactivity and curcumin's known bioactivity, the potential of constructing binary and ternary vanadium-curcumin complex moieties (in the presence of ancillary ligands), conferring appropriately configured biological effects, was probed into through a carefully designed synthetic approach. Stoichiometrically-driven chemical reactivity between V(IV) and curcumin in alcoholic media, in the presence of a strong 2,2'-bipy chelator, led to the isolation and crystallization of compound **1**. This is one of the very rare examples of curcumin bound to a metal ion, in a coordination environment unraveled-confirmed through analytical, spectroscopic techniques and ultimately X-ray crystallography.

The use of the ancillary ligand in the stabilization of the ternary V(IV)-curcumin-(2,2'-bipy) assembly (**1**) suggests that ternary systems of metal ion-natural organic binder chelators, incorporating N,N-aromatic chelators in the complexation process, may lead to isolable crystalline products amenable to full characterization with enhanced hydrolytic stability of bound curcumin, as also reported elsewhere, with the VO^{+2} moiety, and 1,10-phenanthroline and dipyrido[3,2-α:2',3'-c]phenazine as ancillary ligands [**33**]. In that respect, due consideration was given to the herein described synthetic efforts through which the ternary species **1** arose and was further fully characterized analytically, spectroscopically, and crystallographically prior to being employed in biological activity experiments.

The spectroscopic and crystallographic work revealed the presence of an octahedral complex in the solid state. The ternary complex was comprised of curcumin and 2,2'-bipy, with the two ligands introduced in the coordination sphere around V(IV) in a way that the vanadyl oxygen was positioned trans to the water molecule bound to vanadium. This solid state picture was further investigated in solution, with EPR spectroscopy providing further insight into the solution behavior of the species. In fact, the EPR-HYSCORE results suggested the presence of yet another species, with the nitrogen donor anchors of the involved ligands positioned differently from the originally determined crystallographic arrangement in the solid state. The poten-

tial of an equilibrium between conformers of the ternary complex arising upon dissolution of the complex rose prominently. To that end, a tedious yet detailed and comprehensive theoretical work involving diversely configured DFT calculations revealed the energetics of such a transformation that could be taking place, with the cis-conformer lying lower in energy that the trans-conformer observed crystallographically in the solid state (**Table S2**). The details of such a potential conformational equilibrium in solution for the title complex stands in consonance to the suggestions of EPR spectroscopy and sheds further light into that behavior of such species containing V(IV) bound to two different ligands in an octahedral arrangement. The presence of bound water in the coordination sphere of V(IV) introduces conformational diversity in the coordination sphere configuration with the bulk of the organic chelator ligands measuring up to the labile monodentate inorganic water molecule in a conversion process (**Fig. S1B**) with cis- and trans-conformers emerging as participants in any further (bio)chemical reactivity pursued (vide infra). The specifics of such a transformation are quite revealing in projecting a well-defined specific energy profile of intermediates arising in the process (**Fig. S1C**), thereby signifying the importance of a comprehensive investigation of the solid-state and solution behavior of species complemented by theoretical DFT calculations.

4.2 The biological reactivity in a well-defined cellular environment

The investigated biological activity of **1** is a direct consequence of its structural composition, appropriately formulated by the organic chelator moieties curcumin and 2,2'-bipy. The presence of curcumin in the coordination sphere of vanadium signifies the potential of that natural binder to influence metal ionic activity at the biological level. Albeit difficult, at this point, to quantify the contribution of the aromatic chelator 2,2'-bipy to the bioactivity of vanadium relative to that of curcumin, the presence of the latter provides an opportunity to focus on that natural product exerting metal-linked action at the cellular level.

Curcumin has been an extensively used food additive, mainly in India and Southeast Asia, for many centuries. However, its safety and toxicity has been contradictory and extensively conjectured. To our knowledge, there have been clinical studies in phase I conducted on humans, demonstrating curcumin toxicity. The results from a number of preclinical studies have demonstrated that curcumin may be helpful to the prevention and/or treatment of a spectrum of diseases, including Alzheimer's Disease (AD), cancer, cystic fibrosis and inflammatory diseases [**105**]. A dose-dependent investigation was also conducted in order to specify the maximum tolerated dose and safety of a single dose of standardized powder extract of uniformly milled curcumin. Curcumin tolerance at high single oral doses appears to be excellent and was considered safe for humans even (surprisingly-unexpectedly) at single oral administration doses as high as 12 g/day [**106**]. Only minimal toxicity experienced by participating subjects [seven out of twenty-four subjects (30%)] in relevant studies appeared to be dose-dependent. A plethora of a) biological, beneficial, therapeutic properties, including anti-oxidant, anti-inflammatory, anti-cancer activity, anti-HIV activity [**107,108**], or b) detrimental activity-effects were attributed to curcumin, including hepatoxicity, genotoxicity, and others [**109-112**]. Moreover, it's worth noting that despite the paradox of curcumin displaying selective toxicity toward cancer cells, without influencing healthy cells, *in vitro* research demonstrated that curcumin can di-

rect healthy human T cells toward apoptosis at a rate similar to that of cancerous leukemia cells [**109**]. A 90-day administration of curcumin to rats showed that overdose or long term supplementation of curcumin could generate oxidative stress, inflammation, and metabolic disorders, probably causing liver damage [**58**]. An extremely porous bio-Metal-Organic Framework (MOF), medi-MOF-1, was also synthesized from zinc, and a potential therapeutic agent with curcumin arose. The Zn-based MOF demonstrated similar cell growth inhibitory performance through the MTT assay against pancreatic cancer cells (BxPC-3) and it was proposed as a potential drug for biomedical applications [**58**].

The anti-oxidant activity of many agents (compounds), including metal–curcumin complexes, has attracted considerable attention in the preventive and protective treatment of many diseases, such as neurodegenerative diseases and others, e.g. scavenging reactive oxygen species (ROS), blocking Aβ-aggregation, and chelating neuro-toxic metal ions. In this respect, it is well-established that curcumin is able to act as a powerful antioxidant by efficiently scavenging free radicals, i.e. ROS. As a reasonable (logical) consequence, several metal-curcumin compounds have been synthesized in an attempt to exploit their possible antioxidant capacity. To that end, antioxidant properties were reported for curcumin complexes of gallium, indium and vanadyl ions [**113,114**], as well as manganese [**115**], and copper [**116**]. The collective work shows that the behavior of the two compounds (curcumin and the title compound **1**) appears to be one reflecting strong antioxidant agents. That, by all means, does not necessarily mean that a dose-dependent concentration effect applies to all concentrations tested, from low to high ones. It appears, that at low concentrations (1-25 μM), the effects observed are commensurate with the antioxidant behavior of the two compounds, with compound **1** being a stronger antioxidant agent than curcumin (under the employed experimental conditions). When, however, the concentration rises to 40 and 50 μM, i.e. beyond a certain threshold concentration (which was discovered as a result of the experimental process in this work), the two compounds turn to pro-oxidant behavior, thus generating ROS species.

Oxidative stress is considered one of the major causes of DNA damage. Reactive oxygen species, generated during cell metabolism by various agents, could attack the DNA base guanine, forming 8-OHdG lesions, known to possess mutagenic properties, thereby having 8-OHdG routinely used as a biomarker for carcinogenesis [**117**]. A number of studies are being currently conducted on transition metal complexes, other than cisplatin, targeting the discovery of more efficient and less toxic anticancer agents. In that respect, knowledge and delineation of the binding mode(s) of various metal complexes, candidates for chemotherapeutic agents, to nucleic acids, is of crucial significance to the development of such new efficient drugs. Thus, targeted research in the metallo-drug field revolves around the design of compounds preferably targeting DNA binding through non-covalent modes of action, such as binding to major and minor grooves of the double helix, phosphate clamps, and insertion or intercalation [**118-121**]. However, whereas groove binding modes cause only negligible distortions to the B-form structure of the DNA double helix, the intercalation mode of binding promotes the most dramatic alterations in the DNA structure. A crucial factor influencing the binding mode is molecular structure, e.g. extended planar aromatic rings capable of interposing between

paired DNA bases through π-stacking, thereby inducing considerable unwinding, lengthening and destabilization of the double helix [**122,123**].

Although previous in *vitro* experiments had demonstrated that curcumin alone may cause DNA damage to human cells in both peripheral blood lymphocytes [**124**], and gastric mucosal cells [**125**], recent work using similar doses of curcumin did not report DNA damage caused by curcumin to T cells [**126**]. The authors of the study on T cells attributed this discrepancy to the different populations of cells used in the two experiments and perhaps the different methods used in testing DNA damage [**104**]. Moreover, another *in vitro* study conducted on a human fibrosarcoma cell line reported evidence of DNA damage initiated at low curcumin concentrations in the range 3-8 μM, whereas apoptosis was stimulated at concentrations ~10 μM [**127**]. The *in vitro* experiments in the present study, examining the direct effect of both curcumin and ternary compound **1**, showed DNA degradation at curcumin concentrations >25 μM (**Fig.14A-B**). An anisotropic interaction with the DNA helical structure of two new heterolepticpentacoordinatedZn(II) complexes,containing 4,4´-disubstituted 2,2´-bipyridines and curcumin as an ancillary ligand, has been demonstrated. This analysis shows that the interaction mode of curcumin with DNA in the double helix favors their alignment perpendicular to the DNA axis, suggesting partial inter-base intercalation of these Zn(II) complexes [**128**]. Given the composition and formulation of the coordination sphere of V(IV) in the presence of 2,2'-bipy and curcumin, it is not unlikely that a similar interactive mode, encompassing intercalation and/or groove binding, with DNA evolves through chemical reactivity with **1**. Further work on the issue, taking into consideration the influence-contribution of both ligands to the activity of **1**, is currently ongoing in our lab. Overall, the collective biological behavior of the title compound reflects its vanadium-heteroligand complex nature supported by the spectroscopic and theoretical data.

5. Conclusions

The need to develop efficient natural product-containing drugs counteracting pathophysiological conditions led to the synthetic exploration of the ternary V(IV)-curcumin-(2,2'-bipy) system, which led to the isolation of an unusual ternary complex of vanadium $[VO(C_{21}H_{19}O_6)(C_{10}H_8N_2)(H_2O)]_2(SO_4)\cdot 2CH_3OH\cdot 3H_2O$ **(1)**. The detailed physicochemical characterization of the fundamental assembly in **1**a) projected a well-defined coordination environment for V(IV), containing a stabilized curcumin moiety and an ancillary aromatic chelator (2,2'-bipy), all important ingredients in an optimally configured environment of soluble-bioavailable curcumin bio-activity, and b) provided insight into key attributes of the formulated ternary vanado-species, in the solid-state and in solution, supported by analytical, crystallographic, spectroscopic and theoretical studies, further enabling its employment in biological studies relevant to the probe of the antioxidant potential of curcumin. The ternary V(IV)-curcumin-(2,2'-bipy) compound **1**exhibits significant anti-ROS/anti-oxidant activity in yeast cells, in fact reflecting greater potential than curcumin itself. Counter-ROS activity emerges significantly even at very low levels (2.5 μM). Compound **1** was also able to lower MDA levels both inside the cells (in the range 5-25 μM) and in the extracellular growth medium (2.5 μM). Furthermore, the title compound could be considered non-toxic at levels up to 10μM. It does not inhibit cell metabolism by

comparison to curcumin, as proven through the FDA-lytic activity. More in-depth work, however, is needed to delineate the *in vitro* and *in vivo* action of **1** on DNA, as *in vitro* experiments indicate potential genotoxicity. The effect on DNA may be attributed to a possible intercalation mode of action rather than an alteration of the cellular oxidative status, which seems to be improved. Collectively, the experimental results provide a global picture for the biological activity of curcumin, which upon vanadium coordination in the presence of 2,2'-bipy delivers biological activity, thereby enhancing its antioxidant character and setting the basis for the development of new metal-complexed curcumin pharmaceuticals capable of counteracting (sub)cellular pathophysiologies.

Appendix A. Supplementary data

CCDC 1567352 (**1**) contains the supplementary crystallographic data for this paper. These data can be obtained free of charge via www.ccdc.cam.ac.uk/conts/retrieving.html (or from the Cambridge Crystallographic Data Centre, 12 Union Road, Cambridge CB21EZ, UK; fax: (+44) 1223-336-033; or deposit@ccde.cam.ac.uk).

Abbreviation list

Aβ	Amyloid-*β*
AD	Alzheimer's Disease
PDT	Photodynamic therapy
2,2'-bipy	2,2'-bipyridine
UV-Vis	UV-visible
ESI-MS	Electrospray Spray Ionization mass spectrum
FT-IR	FT-Infrared
TGA	Thermogravimetric analysis
EPR	Electron Paramagnetic Resonance
DFT	Density Functional Theory
DOS	Density of States
NEB	Nudged Elastic Band
DMSO-d_6	Deuterated dimethyl sulfoxide
FDA	Fluorescein diacetate
HYSCORE	Hyperfine sublevel correlation spectroscopy
S. cerevisiae	*Saccharomyces cerevisiae*
MDA	Malondialdehyde
TCA	Trichloroacetic acid
TBA	Thiobarbituric acid
ROS	Reactive oxygen species

NBT	Nitrobluetetrazolium chloride
dsDNA	Double-stranded DNA
CT-dsDNA	Calf thymus dsDNA
EtBr	Ethidium bromide
LMCT	Ligand to metal charge transfer
CHEQ	Chelation enhancement of quenching
SEM	Scanning Electron Microscopy
PAS	Principal axis system
HFI	Hyperfine interaction
pDNA	plasmidDNA

Acknowledgments

The work of EH was supported by the IKY Fellowships of Excellence for Postgraduate studies in Greece – Siemens Program 2016-2017. TP acknowledges use of High Performance Computing (HPC) computational facilities provided by the Faculty of Science and Engineering, University of Chester, U.K. E.H. and T.P. acknowledge fruitful discussions with Dr. Spyridon Hadjispyrou during the initial stage of this work.

Conflict of interest

All authors would like to declare that there are no conflicts of interest.

References

1 A.Valentini, F.Conforti, A.Crispini, A.De Martino, R.Condello, C.Stellitano, G. Rotilio, M. Ghedini, G. Federici, S.Bernardini, D.Pucci, J. Med. Chem.52 (2009) 484−491.

2 D. Pucci, R. Bloise, A. Bellusci, S. Bernardini, M. Ghedini, S. Pirillo, A. Valentini, A. Crispini, J. Inorg. Biochem.101 (2007) 1013−1022.

3 E. Ferrari, S. Lazzari, G. Marverti, F. Pignedoli, F. Spagnolo, M. Saladini, Bioorg. Med. Chem. 17 (2009) 3043−3052.

4 X. Y.-M. Song, J.-P.Xu, L. Ding, Q. Hou, J.-W. Liu, Z.- L. Zhu, J. Inorg. Biochem. 103 (2009) 396−400.

5 S. Çıkrıkçı, E. Mozioğlu, H. Yılmaz, Rec. Nat. Prod. 2 (2008) 19–24.

6 H. Hatcher, R. Planalp, J. Cho, F. M. Torti, S. V. Torti, Cell. Mol. Life Sci. 65 (2008) 1631–1652.

7 G. Began, E. Sudharshan, K. U. Sankar, A. G. A. Rao, J. Agric. Food Chem. 47 (1999) 4992–4998.

8 P. H. Bong, Bull. Korean Chem. Soc. 21 (2000) 81–86.

9 P. Anand, S. G. Thomas, A. B. Kunnumakkara, C. Sundaram, K. B. Harikumar, B. Sung, S. T. Tharakan, K. Misra, I. K. Priyadarsini, K. N. Rajasekharan, B. B. Aggarwal, Biochem. Pharmacol. 76 (2008) 1590−1611.

10 B. B. Aggarwal, C. Sundaram, N. Malani, H. Ichikawa, Adv. Exp. Med. Biol. 595 (2007) 1−75.

11 G. B. Mahady, S. L. Pendland, G. Yun, Z. Z. Lu, Anticancer Res. 22 (2002) 4179–4181.

12 Y. Sugiyama, S. Kawakishi, T. Osawa, Biochem. Pharmacol. 52 (1996) 519–525.

13 A. J. Ruby, G. Kuttan, K. D. Babu, K. N. Rajasekharan, R. Kuttan, Cancer Lett. 94 (1995) 79–83.

14 W. C. Jordan, C. R.Drew, J. Natl. Med. Assoc. 88 (1996) 333–335.

15 F. Yang, P. L. G. P. Lim, A. N. Begum, O. J. Ubeda, M. R. Simmons, S. S. Ambegaokar, P. Chen, R. Kayed, C. G. Glabe, S. A. Frautschy, G. M. Cole, J. Biol. Chem. 280 (2005) 5892−5901.

16 M. Garcia-Alloza, L. A. Borrelli, A. Rozkalne, B. T. Hyman, B. J. Bacskai, J. Neurochem. 102 (2007) 1095−1104.

17 E. Delaey, F. V. Laar, D. De Vos, A. Kamuhabwa, P. Jacobs, P. De Witte, J. Photochem. Photobiol. B 55 (2000) 27-36.

18 D. E. Dolmans, D. Fukumura, R. K. Jain, Nat. Rev. Cancer 3 (2003) 380-387.

19 T. A. Dahl, P. Bilski, K. J. Reszka and C. F. Chignell, J. Photochem. Photobiol. 59 (1994) 290-294.

20 S. Chakraborti, L. Das, N. Kapoor, A. Das, V. Dwivedi, A. Poddar, G. Chakraborti, M. Janik, G. Basu, D. Panda, P. Chakrabarti, A. Surolia, B. Bhattacharyya, J. Med. Chem. 54 (2011) 6183-6196.

21 B. Banik, K. Somyajit, G. Nagaraju, A. R. Chakravarty, Dalton Trans. 43 (2014) 13358-13369.

22 S. Qureshi, A. H. Shah, A. M. Ageel, Planta Med. 58 (1992) 124–127.

23 C. D. Lao, M. T. Ruffin, D. Normolle, D. D. Heath, S. I. Murray, J. M. Bailey, M. E. Boggs, J. Crowell, C. L. Rock, D. E. Brenner, Altern. Med. 6 (2006) 10.

24 R. A. Sharma, W. P. Steward, A. J. Gescher, Adv. Exp. Med. Biol.595 (2007) 453-470.

25 L. Shen, H. F. Ji, Trends Mol. Med. 18 (2012) 138-144.

26 Y.-J. Wang, M.-H. Pan, A.-L. Cheng, L.-I. Lin, Y.-S. Ho, C.-Y. Hsieh, J.-K. Lin, J. Pharm. Biomed. Anal. 15 (1997) 1867-1876.

27 P. Anand, A. B. Kunnumakkara, R. A. Newman, B. B. Aggarwal, Mol. Pharm. 4 (2007) 807–818.

28 B. Antony, B. Merina, V. S. Iyer, N. Judy, K. Lennertz, S. A. Joyal, Ind. J. Pharm. Sci. 70 (2008) 445–449.

29 F. Zhang, G. K. Koh, D. P. Jeansonne, J. Hollingworth, P. S. Russo, G. Vicente, R. W. Stout, Z. Liu, J. Pharm. Sci. 100 (2011) 2778–2789.

30 N. K. Gupta, V. K. Dixit, J. Pharm. Sci.100 (2011) 1987–1995.

31 P. Anand, S. G. Thomas, A. B. Kunnumakkara, C. Sundaram, K. B. Harikumar, B. Sung, S. T. Tharakan, K. Misra, I. K. Priyadarsini, K. N. Rajasekharan, B. B. Aggarwal, Biochem. Pharmacol. 76 (2008) 1590−1611.

32 B. B. Aggarwal, C. Sundaram, N. Malani, H. Ichikawa, Adv. Exp. Med. Biol. 595 (2007) 1−75.

33 S. Banerjee, P. Prasad, A. Hussain, I. Khan, P. Kondaiah, A. R. Chakravarty, Chem. Commun. 48 (2012) 7702-7704.

34 D. Pucci, T. Bellini, A. Crispini, I. D'Agnano, P. F. Liguori, P. Garcia-Orduña, S. Pirillo, A. Valentini, G. Zanchettab, Med. Chem. Commun. 3 (2012) 462-468.

35 F. Kuhlwein, K. Polborn, W. Beck, Z. Anorg. Allg. Chem. 623 (1997) 1211-1219.

36 D. C. Crans, J. J. Smee, E. Gaidamauskas, L. Yang, Chem. Rev. 104 (2004) 849-902.

37 G. R.Willsky, K. Halvorsen , M. E. Godzala, L. H. Chi, M. J. Most, P. Kaszynski, D. C. Crans, A. B. Goldfine , P. J. Kostyniak, Metallomics 5 (2013) 1491-1502.

38 A. Tesmar, D. Wyrzykowski, R. Kruszyński, K. Niska, I. Inkielewicz-Stępniak, J. Drzeżdżon, D. Jacewicz, L. Chmurzyński, Biometals 30 (2017) 261–275.

39 A. B. Gordon, J. F. Berry, J. Chem. Educ. 85 (2008) 532-536.

40 S. Stoll, A. Schweiger, J. Magn. Reson. 178 (2006) 42-55.

41 G. Kresse, J. Furthmüller, Phys. Rev. B 54 (1996) 11169-11186.

42 J. P. Perdew, K. Burke, M. Ernzerhof, Phys. Rev. Lett. 78 (1997) 1396.

43 S. Grimme, J. Comp. Chem. 27 (2006) 1787-1799.

44 P. E. Blöchl, Phys. Rev. B 50 (1994) 17953-17979.

45 a) G. Kresse, D. Joubert, Phys. Rev. B 59 (1999) 1758-1775.
b) S. Smidstrup, A. Pedersen, K. Stokbro, H. Jónsson, J. Chem. Physics 140 (2014)214106.

46 K. Momma, F. Izumi, J. Appl. Crystallogr. 44 (2011) 1272-1276.

47 Bruker Analytical X-ray Systems, Inc. Apex2, Version 2 User Manual, M86-E01078, Madison, WI (2006).

48 Siemens Industrial Automation, Inc. SADABS: Area-Detector Absorption Correction; Madison, WI (1996).

49 P. W. Betteridge, J. R. Carruthers, R. I. Cooper, K. Prout, D. J. Watkin, J. Appl. Cryst. 36 (2003) 1487.

50 L. Palatinus, G. Chapuis, J. Appl. Cryst.40 (2007) 786-790.

51 DIAMOND – Crystal and Molecular Structure Visualization, Ver. 3.1c, Crystal Impact, Bonn, Germany (2006).

52 P. Verma, J.Dyckmans, H.Militz, C.Mai, Appl. Microbiol.Biotechnol. 80 (2008) 125−133.

53 L. J. Niedernhofer, J. S. Daniels, C. A. Rouzer, R. E. Greene, L. J. Marnett,J. Biol. Chem. 278 (2003) 31426-31433.

54 K. Giannousi, G. Sarafidis, S. Mourdikoudis, A. Pantazaki, C. Dendrinou-Samara, Inorg. Chem. 53 (2014) 9657-9666.

55 S. Wanninger, V. Lorenz, A. Subhan, F.T. Edelmann, Chem. Soc. Rev. 44 (2015) 4986-5002.

56 S. Banerjee, I. Pant, I. Khan, P. Prasad, A. Hussain, P. Kondaiah, A.R. Chakravarty, Dalton Trans. 44 (2015) 4108-4122.

57 U. Bhattacharyya, B. Kumar, A. Garai, A. Bhattacharyya, A. Kumar, S. Banerjee, P. Kondaiah, A.R. Chakravarty, Inorg. Chem. 56 (2017) 12457-12468.

58 H. Su, F. Sun, J. Jia, H. He, A. Wang, G.Zhu, Chem. Commun. 51 (2015) 5774-5777.

59 K. Lawrence, S.E. Flower, G. Kociok-Kohn, C.G. Frost, T.D. James, Anal. Methods. 4 (2012) 2215-2217.

60 D. Pucci, T. Bellini, A. Crispini, I. D'Agnano, P. F. Liguori, P. Garcia-Orduña, S. Pirillo, A. Valentini, G. Zanchetta, Med. Chem. Commun. 3 (2012) 462–468.

61 A. Hussain, K. Somyajit, B. Banik, S. Banerjee, G. Nagaraju, A.R. Chakravarty, Dalton Trans. 42 (2013) 182-195.

62 F. Caruso, M. Rossi, A. Benson, C. Opazo, D. Freedman, E. Monti, M.B. Gariboldi, J. Shaulky, F. Marchetti, R. Pettinari, C. Pettinari, J. Med. Chem. 55 (2012) 1072–1081.

63 F. Kühlwein, K. Polborn, W. Beck, Z. Anorg. Allg. Chem. 623 (1997) 1211–1219.

64 C. Triantis, T. Tsotakos, C. Tsoukalas, M. Sagnou, C. Raptopoulou, A. Terzis, V. Psycharis, M. Pelecanou, I. Pirmettis, M. Papadopoulos, Inorg. Chem. 52 (2013) 12995–13003.

65 R. Pettinari, F. Marchetti, F. Condello, C. Pettinari, G. Lupidi, R. Scopelliti, S. Mukhopadhyay, T. Riedel, P.J. Dyson, Organometallics. 33 (2014) 3709−3715.

66 E. Halevas, O. Tsave, M.P. Yavropoulou, A. Hatzidimitriou, J.G. Yovos, V. Psycharis, C. Gabriel, A. Salifoglou, J.Inorg. Biochem. 147 (2015) 99-115.

67 L. D. Frederickson, D. M. Hausen, Anal. Chem. 35 (1963) 818–827.

68 G. D. Bajju, P. Sharma, A. Kapahi, M. Bhagat, S.Kundan,D. Gupta, J. Inorg. Chem. 2013, Article ID 982965, 11 pages.

69 R. Díaz-Torres, M. Menelaou, O. Roubeau, A. Sorrenti,G. Brandariz-de-Pedro, E. C. Sañudo, S. J. Teat, J. Fraxedas, E. Ruizaf, N. Aliaga-Alcalde, Chem. Sci.7 (2016) 2793–2803.

70 A. K. Boudalis, V. Nastopoulos, S. P. Perlepes, C. P. Raptopoulou, A. Terzis, Trans. Met. Chem. 26 (2001) 276-281.

71 B. Unterhalt, Z. Lebensm. Unters. Forsch. 170 (1980) 425-428.

72 F. Payton, P. Sandusky, W. L. Alworth, J. Nat. Prod. 70 (2007) 143-146.

73 W.-Z. Shen, G. Trötscher-Kaus, B. Lippert, Dalton Trans.(2009) 8203-8214.

74 L. Shen, H.-F. Ji, Spectrochim. Acta-Part A67 (2007) 619.

75 F. Zsila, Z. Bikadi, M. Simonyi, Biochem. Biophys. Res. Commun. 301 (2003) 776–782.

76 C. F. Chignell, P. Bilski, K. J. Reszka, A. N. Motten, R. H. Sik, T. A. Dhal, Photochem. Photobiol.59 (1994) 295–302.

77 S. M. Khopde, K. I. Priyadarsini, D. K. Palit, T. Mukherjee, Photochem. Photobiol. 72 (2000) 625–631.

78 L. Nardo, R. Paderno, A. Andreoni, M. Mason, T. Haukvik, H. H. Tonnesen, Spectroscopy 22 (2008) 187–198.

79 P. H. Bong, Bull. Kor. Chem. Soc.21 (2000) 81–86.

80 R. Adhikary, P. Mukherjee, T. W. Kee, J. W. Petrich, J. Phys. Chem. B 113 (2009) 5255–5261.

81 M. Bernabe-Pineda, M. T. Ramirez-Silva, M. Romer-Romo, E. Gonzalez-Vergara, A. Rojas-Hernandez, Spectrochim. Acta A 60 (2004) 1091–1097.

82 M. Griesser, V. Pistis, T. I. Suzuki, N. Tejera, D. A. Pratt, C. Schneider, J. Biol. Chem. 286 (2011) 1114-1124.

83 O. N. Gordon, P. B. Luis, H. O. Sintim, C. Schneider, J. Biol. Chem. 290 (2015) 4817-4828.

84 N. Aliaga-Alcalde, P. Marqués-Gallego, M. Kraaijkamp, C. Herranz-Lancho, H. den Dulk, H. Gorner, O. Roubeau, S. J. Teat, T. Weyhermüller, J. Reedijk, Inorg. Chem. 49 (2010) 9655–9663.

85 M. Menelaou, T. Weyhermüller, M. Soler, N. Aliaga-Alcalde, Polyhedron 52 (2013) 398–405.

86 M. Menelaou, F. Ouharrou, L. Rodríguez, O. Roubeau, S. J. Teat, N. Aliaga-Alcalde, Chem.-Eur. J.18 (2012) 11545–11549.

87 N. Aliaga-Alcalde, L. Rodríguez, Inorg. Chim. Acta380 (2012) 187–193.

88 K. Toshima, R. Takano, T. Ozawa, S. Matsumura, Chem. Commun. (2002) 212-213.

89 K. I. Priyadarsini, J. Photochem. Photobiol. C: Photochem. Rev. 10 (2009) 81–95.

90 N. Aliaga-Alcalde, L. Rodríguez, M. Ferbinteanu, P. Hofer, T. Weyhermüller, Inorg. Chem.51 (2012) 864–873.

91 N. F. Chilton, R. P. Anderson, L. D. Turner, A. Soncini, K. S. Murray, J. Comput. Chem. 34 (2013) 1164–1175.

92 V. Murgia, E. M. Farfán Torres, J. C. Gottifredi, E. L. Sham, Applied Catalysis A: General 312 (2006) 134–143.

93 C. Duval, "Inorganic Thermogravimetric Analysis", Second and Revised Edition, Elsevier Publishing Co., Amsterdam (1963).

94 T. Tashiro, J. Chem. Soc. Japan52 (1931) 727-729.

95 J. Selbin, Chem. Rev.65 (1965) 153–175.

96 A. K. Yadava, H. S. Yadav, U. S. Yadav, D. P. Rao, Turk. J. Chem.36 (2012) 624–630.

97 K.S.Patel, J. Inorg. Nucl. Chem.43 (1981) 667-669.

98 N. Noshiranzadeh, M. Emami, R. Bikas, J. Sanchiz, M. Otręba, P. Aleshkevych, T. Lis, Polyhedron 122 (2017) 194-202.

99 A. Schweiger, G. Jeschke, Principles of Pulse Electron Paramagnetic Resonance. 1st Edition. Oxford University Press, 2001.

100 E. J. Reijerse, A. M. Tyryshkin, S. A. Dikanov, J. Magn. Reson. 131 (1998) 295-309.

101 R. LoBrutto, B. J. Hamstra, G. J. Colpas, V. L. Pecoraro, W. D. Frasch, J. Am. Chem. Soc. 120 (1998) 4410-4416.

102 B. Kisrte, H. van Willigen, J. Phys. Chem. 86 (1982) 2743-2749.

103 W. Tang, E. Sanville, G. Henkelman, J. Phys.: Condens. Matter 21 (2009) 084204.

104 L. J. Niedernhofer, J. S. Daniels, C. A. Rouzer, R. E. Greene, L. J. Marnett, J. Biol. Chem.278 (2003) 31426-31433.

105 M. N. Tsolaki, E. Koutsouraki, G. K. Katsipis, P. G. Myserlis, M. A. Chatzithoma, A. A. Pantazaki, Alternative Anti-Infective/Anti-Inflammatory Therapeutic Options for Fighting Alzheimer's Disease.

Bentham eBooks series “Frontiers in Anti-Infective Drug Discovery”, Bentham Science Publishers 6 (2017) 3-161.

106 C. D. Lao, M. T. Ruffin, D. Normolle, D. D. Heath, S. I. Murray, J. M. Bailey, M. E. Boggs, J. Crowell, C. L. Rock, D. E. Brenner, BMC Complement Altern. Med.6 (2006) 10.

107 O. P. Sharma, Biochem. Pharmacol.25 (1976) 1811-1812.

108 R. K. Maheshwari, A. K. Singh, J. Gaddipati, R. C. Srimal, Life Sci.78 (2006) 2081-2087.

109 V. J. Navarro, H. Barnhart, H. L. Bonkovsky, T. Davern, R. J. Fontana, L. Grant, K. R. Reddy, L. B. Seeff, J. Serrano, A. H. Sherker, A. Stolz, J. Talwalkar, M. Vega, R. Vuppalanchi, Hepatology. 60 (2014) 1399-1408.

110 H. F. Lu, J. S. Yang, K. C. Lai, S. C. Hsu, S. C. Hsueh, Y. L. Chen, J. H. Chiang, C. C. Lu, C. Lo, M. D. Yang, J. C. Chung,Neurochem. Res. 34 (2009) 1491-1497.

111 Z. Korwek, A. Bielak-Zmijewska, G. Mosieniak, O. Alster, M. Moreno-Villanueva, A. Burkle, E.Sikora, Mutagenesis 28 (2013) 411-416.

112 P. Qiu, S. Man, J. Li, J. Liu, L. Zhang, P. Yu, W.Gao, J. Agric. Food Chem.64 (2016) 2765-2771.

113 M. Asti, E. Ferrari, S. Croci, G. Atti, S. Rubagotti, M. Iori, P. C. Capponi, A. Zerbini, M. Saladini, A. Versari, Inorg. Chem.53 (2014) 4922–4933.

114 K. Mohammadi, K. H. Thompson, B. O. Patrick, T. Storr, C. Martins, E. Polishchuk, V. G. Yuen, J. H. McNeill and C. Orvig, J. Inorg. Biochem.99 (2005) 2217–2225.

115 Y. Sumanont, Y. Murakami, M. Tohda, O. Vajragupta, H. Watanabe, K. Matsumoto, Biol. Pharm. Bull.30 (2007) 1732–1739.

116 A. Barik, B. Mishra, A. Kunwar, R. M. Kadam, L. Shen, S. Dutta, S. Padhye, A. K. Satpati, H.-Y. Zhang, K. I. Priyadarsini, Eur. J. Med. Chem.42 (2007) 431–439.

117 P. Karihtala, Y. Soini, L. Vaskivuo, R. Bloigu, U. Puistola, Int. J. Gynecol. Cancer19 (2009) 1047–1051.

118 I. Ott, R. Gust, Arch. Pharm. (Weinheim)340 (2007)117-126.

119 M. A. Jakupec, M. Galanski, V. B. Arion, C. G. Hartinger, B. K. Keppler, Dalton Trans. (2008) 183–194.

120 P. C. Bruijnincx, P. J. Sadler, Curr. Opin. Chem. Biol.12 (2008) 197–206.

121 G. Sava, A. Bergamo, P. J. Dyson, Dalton Trans.40 (2011) 9069–9075.

122 B. M. Zeglis, V. C. Pierre, J. K. Barton, Chem. Commun. (2007) 4565–4579.

123 A. Mukherjee, R. Lavery, B. Bagchi, J. T. Hynes, J. Am. Chem. Soc.130 (2008) 9747–9755.

124 J. Blasiak, A. Trzeciak, J. Kowalik, J. Environ. Pathol.Toxicol.Oncol.18 (1999) 271-276.

125 J. Błasiak, A. Trzeciak, E. Małecka-Panas, J. Drzewoski, T. Iwanienko, I. Szumiel, M.Wojewódzka, Teratog. Carcinog. Mutagen.19 (1999) 19-31.

126 Z. Korwek, T. Sewastianik, A. Bielak-Zmijewska, G. Mosieniak, O. Alster, M. Moreno-Villaneuva, A. Burkle, E. Sikora, DNA Repair11 (2012) 864–873.

127 B. Sun, S. M. Ross, O. J. Trask, P. L. Carmichael, M. Dent, A. White, M. E. Andersen, R. A. Clewell, Toxicol. In Vitro(2013) 271877-271887.

128 D. Pucci, T. Bellini, A. Crispini, I. D'Agnano, P. F. Liguori, P. Garcia-Orduña, S. Pirillo, A. Valentini, G. Zanchetta, Med. Chem. Commun.3 (2012) 462-468.

Table 1: Summary of Crystal, Intensity Collection and Refinement Data for $[VO(C_{21}H_{19}O_6)(C_{10}H_8N_2)(H_2O)]_2(SO_4)\cdot 2CH_3OH\cdot 3H_2O$**(1)**.

	1
formula	$C_{64}H_{72}N_4O_{25}SV_2$
molecular mass	1431.23
T, °K	295
radiation type	MoK_a
wavelength, λ (Å)	0.71073
crystal system	monoclinic
space group	C2/c
a (Å)	30.117(4)
b (Å)	15.545(2)
c (Å)	15.940(3)
α, deg	90°
β, deg	116.180(17)°
γ, deg	90°
V, (Å^3)	6696.9(13)
Z	4
D_{calcd} (Mg m^{-3})	1.419
abs.coeff. (μ), mm^{-1}	0.39
range of h,k,l	-36→32, -18→18, 0→19
goodness-of-fit on F^2	1.0000
Measured, independent and observed reflections ($I>2\sigma(I)$)	63113,6203,4457[1]
R	0.064
R_w	0.073

$$R = \frac{\sum \| |F_o| - |F_c| \|}{\sum (|F_o|)}, \; R_w = \sqrt{\sum \left[w(F_o^2 - F_c^2)^2 \right] \Big/ \sum \left[w(F_o^2)^2 \right]}$$

R values are based on F values, R_w values are based on F^2; $w=w' \times [1 - (\Delta F_{obs} / 6 \times \Delta F_{est})^2]^2$

where $w'=[P_0T_0'(x) + P_1T_1'(x) + ... P_{n-1}T_{n-1}'(x)]^{-1}$ and P_i are the coefficients of a Chebychev series in $t_i(x)$, and $x = F_{calc}^2/F_{calc}^2{}_{max}$ $w = (1/4F_{obs}^2) \times 1$

Table 3: Bond lengths [Å] and angles [deg] for $[VO(C_{21}H_{19}O_6)(C_{10}H_8N_2)(H_2O)]_2(SO_4)\cdot 2CH_3OH\cdot 3H_2O$**(1)**.

	Bond length (Å)
V(1)-N(1)	2.128(2)
V(1)-N(2)	2.081(2)
V(1)-O(1)	1.9643(18)
V(1)-O(2)	1.9561(17)
V(1)-O(7)	1.587(2)
V(1)-O(31)	2.308(2)
	Angle (°)
N(1)-V(1)-N(2)	78.02(9)°
N(1)-V(1)-O(1)	91.69(8)°
N(2)-V(1)-O(1)	160.97(11)°
N(1)-V(1)-O(2)	161.13(10)°
N(2)-V(1)-O(2)	94.05(9)°
O(1)-V(1)-O(2)	90.74(8)°
N(1)-V(1)-O(7)	98.16(10)°
N(2)-V(1)-O(7)	97.36(11)°
O(1)-V(1)-O(7)	99.95(9)°
O(2)-V(1)-O(7)	99.84(9)°
N(1)-V(1)-O(8)	79.35(9)°
N(2)-V(1)-O(8)	78.88(10)°
O(1)-V(1)-O(8)	83.53(9)°
O(2)-V(1)-O(8)	82.34(9)°
O(7)-V(1)-O(8)	175.83(9)°

Table 4: Simulation parameters using two coupled ^{14}N nuclei for the spectrum shown in **Fig. 9B** (set 1).

	Tensor[b]	1	2	3	iso	(Euler angles in °)[a]		
						ϕ	θ	ψ
	HFI	–7.32	–5.67	–6.00	–6.33	0	0	0
N1						α	β	γ
	NQI	–1.50	0.65	0.85		0	0	–90
		K =–0.75	η=0.13					
						ϕ	θ	ψ
	HFI	–7.32	–5.67	–6.00	–6.33	0	0	–75
N2						α	β	γ
	NQI	–1.50	0.65	0.85		0	0	–165
		K=–0.75	η=0.13					

[a] Active rotation.

[b] Principal values of tensors in MHz.

Table 5: Simulation parameters using two coupled ^{14}N nuclei for the spectrum shown in **Fig. 9C** (set 2).

	Tensor[b]	1	2	3	iso	(Euler angles in °)[a]		
						ϕ	θ	ψ
	HFI	–7.32	–5.67	–6.00	–6.33	0	0	0
N1						α	β	γ
	NQI	–1.50	0.65	0.85		0	0	–90
		K =–0.75	η=0.13					
						ϕ	θ	ψ
	HFI	1.00	1.20	0.60	0.93	0	0	0
N2						α	β	γ
	NQI	–1.80	0.63	1.17		0	–90	0
		K=–0.90	η=0.30					

[a] Active rotation.

[b] Principal values of tensors in MHz.

Figure Captions

Figure 1: Partially labeled plot of **1**. Hydrogen atoms were omitted for clarity. Color code: V, purple; O, red; N, blue; C, white.

Figure 2: ESI-MS spectrum of **1**.

Figure 3: Solution ^{1}H (**A**) and ^{13}C-NMR (**B**) spectra of **1**inDMSO-d_6.Thepeaks, marked as S, are due to the solvent.

Figure 4: **A.**UV-Visible spectra of **1**(black line) and pure curcumin (red line).
B.Concentration-dependent UV-Visible spectrum of **1** at various(concentrations $>10^{-6}$ M).

Figure 5: Fluorescence spectra of **1**and pure curcumin.

Figure 6: TGA diagram of **1.**

Figure 7: Graph ofμ_{eff} and μ_{eff}*T of **1**with temperature in a field of $\mu_0 H$ = 1 T (10000 Oe).

Figure 8: CW-X-band experimental (solid line) and theoretical (dotted line) EPR spectrum of **1** in frozen methanol/toluene solution. EPR conditions: Temperature 70K, Modulation amplitude5 Gpp, microwave power20 μW, microwave frequency 9.704 GHz.

Figure 9: (**A**) Experimental HYSCORE spectrum of **1** in methanol/toluene frozen solution (1:1) measured at the $g_{\perp}$ observer position, B=336.6 mT.Three spectra measured with τ = 120 ns, τ = 144 ns, and τ = 168 ns are summed in order to reduce the blind spot effect. Experimental parameters: $t_{\pi/2}$ = 16 ns; time increment, Δt = 24 ns (data matrix 180×180). A four-step phase cycle was used to removeunwanted echoes.(**B)** and(**C)** simulations of (**A)** with two different systems (for simulation parameters see text).

Figure 10: (**A**) Total density of states (solid black line) as well as individual contributions from V atoms (red line), O atoms (green line), C atoms (black solid line), N atoms (blue solid line), S atoms (blue dashed line), and H atoms (brown line) for the vanadium-curcumin complex extracted using Density Functional Theory.
(**B**) DOS projected partial charge density of one out of eight vanadium-curcumin complexes included in the simulation unit cell. It corresponds to states between the conduction band minimum and the Fermi level, E_F (**Fig. 10A**). The isosurface was set to a saturation level of 0.01.

Figure 11: The difference in total energy between trans and cis as well as seven intermediate conformers extracted via the NEB method (Section 2.1.9).

Figure 12: Comparative percent fungal growth before (100%) and after exposure of *S. cerevisiae* cells to various concentrations of curcumin and **1**.Yeast cells grown in MMS medium for 24 h with several concentrations (2.5, 5, 10, 20, 25, 40, and 50 μM) of pure curcumin (orange bars) and **1** (red bars). Growth has been determinedthrough turbidity measurements (A_{600}). Both pure curcumin (black line) and compound **1** (red line) inhibitedyeastgrowth with increasing concentrations, with**1**inhibiting cell growth to a greater extent than pure curcumin. Statistical significance compared to control: $p>0.05$ (ns), $p<0.05$ (*), $p<0.01$ (**) and $p<0.001$(***).

Figure 13: **(A)**Viability of *S. cerevisiae* cells in the absence of any compound (%) and presence of various concentrations of curcumin and compound **1**. Yeast cell viability at various concentrations (2.5, 5, 10, 20, 25, 40, and 50 μM) of pure curcumin (orange bars) and compound **1** (red bars) compared to control, as determined through enzymatic hydrolysis of FDA for 1 h at 37 ^{o}C.**(B)**Viability of *S. cerevisiae* cells in the presence of curcumin 5 μM (green line) and 25 μM (turquoise), 5 μM (blue line) and 25 μM (fuchsia line) of compound **1**,and in the ab-

sence of any compound (control, red line). Fluorescence was measured at λ_{ex}= 455 nm and λ_{em}(max) = 515 nm. The fluorescence of the hydrolyzed product was measured after excitation at λ_{ex} = 494 nm and emission at wavelengths between λ_{em}500-560 nm, with a peak at about 523 nm. Results, as graphed in **(B)**,show that pure curcumin disturbs significantly yeast cell metabolic activity, as that is reflected into decreased enzymatic hydrolysis. Statistical significance compared to control: p>0.05 (ns), p<0.05 (*), p<0.01 (**) and p<0.001(***).

Figure 14: Levels of hyper-oxidized lipid products, namely MDA, generated by fungal *S. cerevisiae* cells exposed to various concentrations of curcumin and compound **1** intracellularly **(A)**,and secreted extracellularly**(B)**. Cells were grown in the presence of several concentrations (2.5, 5, 10, 20, 25, 40, and 50 μM) of pure curcumin (orange bars) or compound **1** (red bars), and centrifuged. The cells were boiled in a lysis buffer containing100 mMNaCl, 1% (w/v) SDS, 2% (v/v) Triton X-100, 10 mMTris-HCl pH 8.00, and 1mM EDTA followed by ultrasound treatment. A volume of 500μL of a 0.67% TBA, 20% (w/v) buffer,was added to the same volume of lysate or growth medium, and the colored product was measured at 535 nm. The graphs (orange for pure curcumin, red for compound **1**) show no significant changes in intracellular MDA concentration, with the exception of 5 μM of both compounds (-25% compared to control), for tested concentrations in the range from 5 to 25 μM of both compounds, whereas increased MDA levelswere observed extracellularly for both pure curcumin and compound **1**. Statistical significance compared to control: p>0.05 (ns), p<0.05 (*), p<0.01 (**) and p<0.001(***).

Figure 15: Intracellular levels of free ROS ($O_2^{-\bullet}$)in yeast cells. Cells were grown in the presence of several concentrations (2.5, 5, 10, 20, 25, 40, and 50 μM) of curcumin (orange bars) or compound **1** (red bars) and centrifuged. The recovered cells were dispersed in100 μL of MMS growth medium and 500 μL of 1 $mg \cdot mL^{-1}$NBT. After the reaction, the formazan product was dissolved and the absorbancewas measured at 575 nm. Free ROS decreased significantly in the presence of a wide range of compound **1** concentrations (up to 90% drop at 25 μM).Statistical significance compared to control: p>0.05 (ns), p<0.05 (*), p<0.01 (**) and p<0.001(***).

Figure 16: **(A)** Agarose (1%) gel electrophoresis of CT-dsDNA. Each sample containing 3 μg of CT-dsDNAwas treated with curcumin or compound **1** at 37°C for 1 h;

Lane M: Molecular weight markers, 1 kb ladders. **Lanes 1-8**:CT-dsDNA treated with 2.5, 5, 10, 20, 25, 40, and 50 μM of pure curcumin. **Lane C:** control, CT-dsDNAwithout treatment; **Lanes 1´-8´**:CT-dsDNA treated with the same concentrations ofcompound **1**.

(B) Quantification of DNA integrity (%) of the main band of the CT-dsDNAfollowing treatment in vitro with various concentrations ranging from 2.5, 5, 10, 15, 20, 25, 40, and 50 μM of curcumin (**Lanes 1-8**) and compound **1**(**Lanes 1´-8´**) of the agarose gel **Fig. 16A**.Statistical significance compared to control: $p>0.05$ (ns), $p<0.05$ (*), $p<0.01$ (**) and $p<0.001$(***).

(**C**) Agarose (1%) gel electrophoretic pattern of an (EtBr)-stained mixture of supercoiled (S) and relaxed (R) pDNA (pUC18) after 1 h of electrophoresis. S represents the supercoiled, R the relaxed, D the dimer, M the multimer, and L the linear form of pDNA (pUC18). Each sample containing 3 μg of pDNAwas treated with curcumin orcompound **1**at 37 ºC for 1 h; **Lanes 1-7:**plasmid DNA treated with 2.5, 5, 10, 15, 20, 25, and 50 μM of curcumin.**Lane C**: control, plasmid DNA without treatment.**Lanes 1´-7´**: plasmid DNA treated with the same concentrations of compound **1**.

Figures

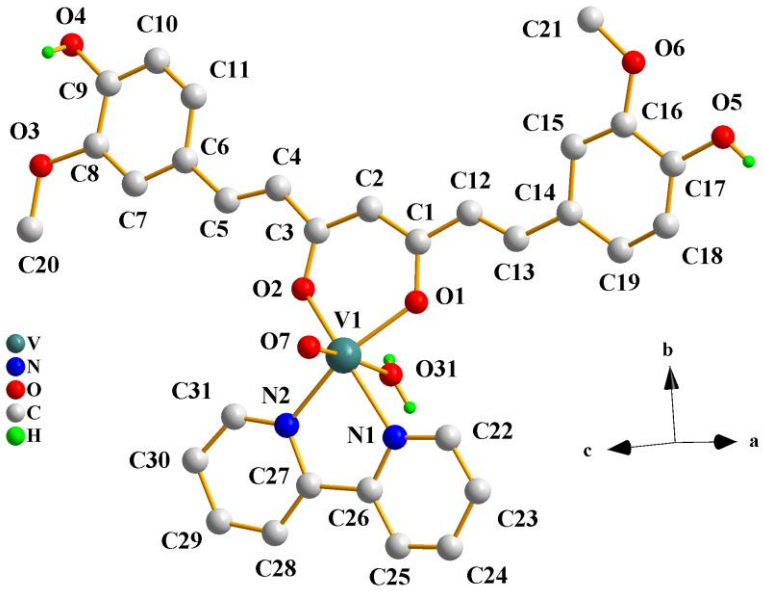

Figure 1

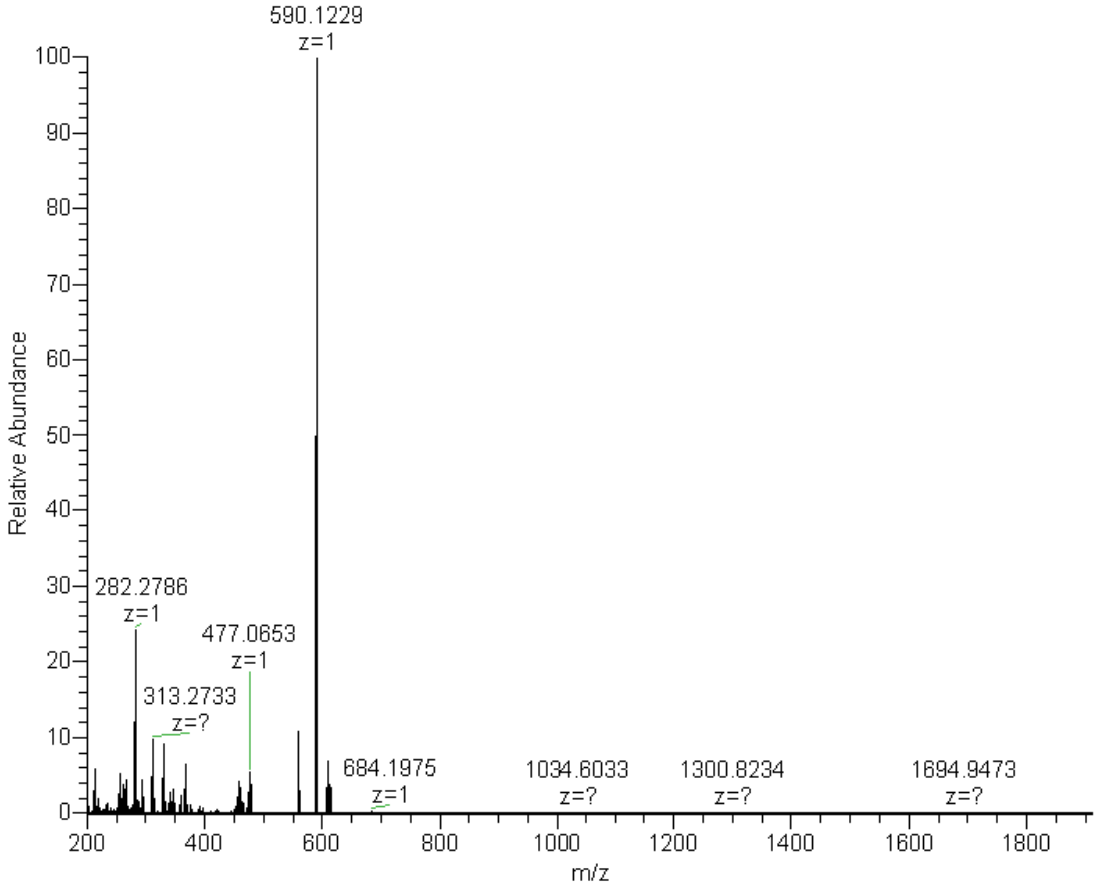

Figure 2

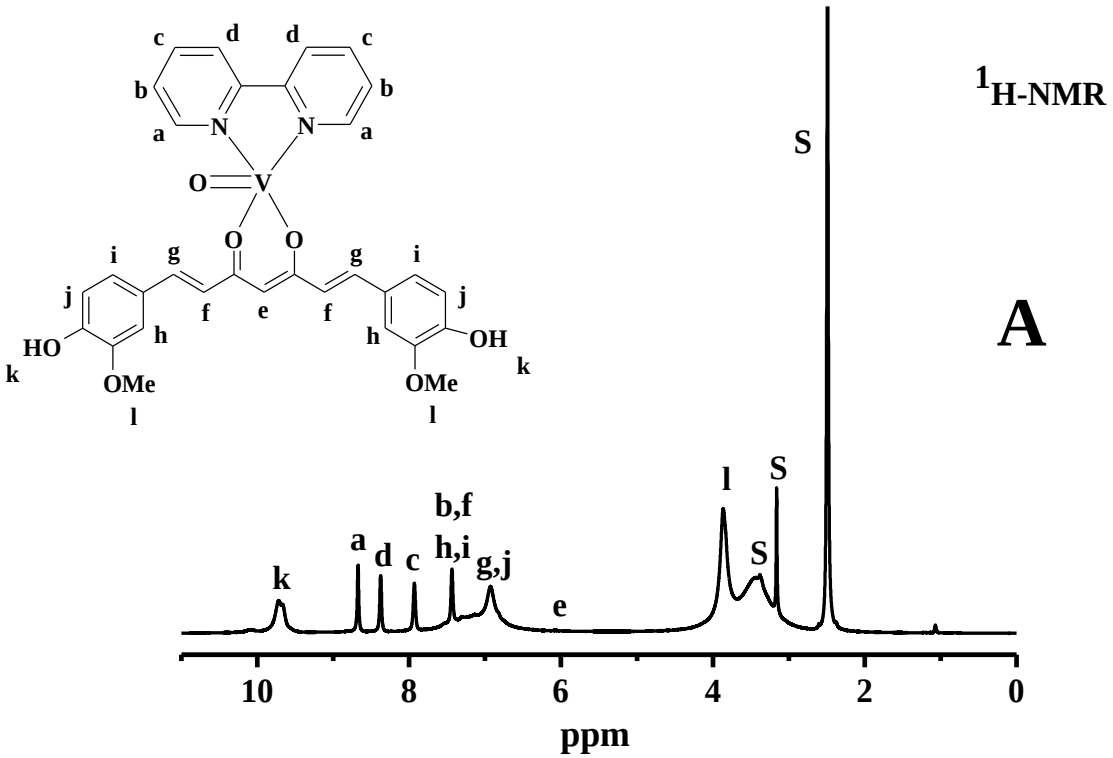
1H-NMR
A
S
l
S
S
b,f
a
d
c
h,i
g,j
k
e
10
8
6
4
2
0
ppm

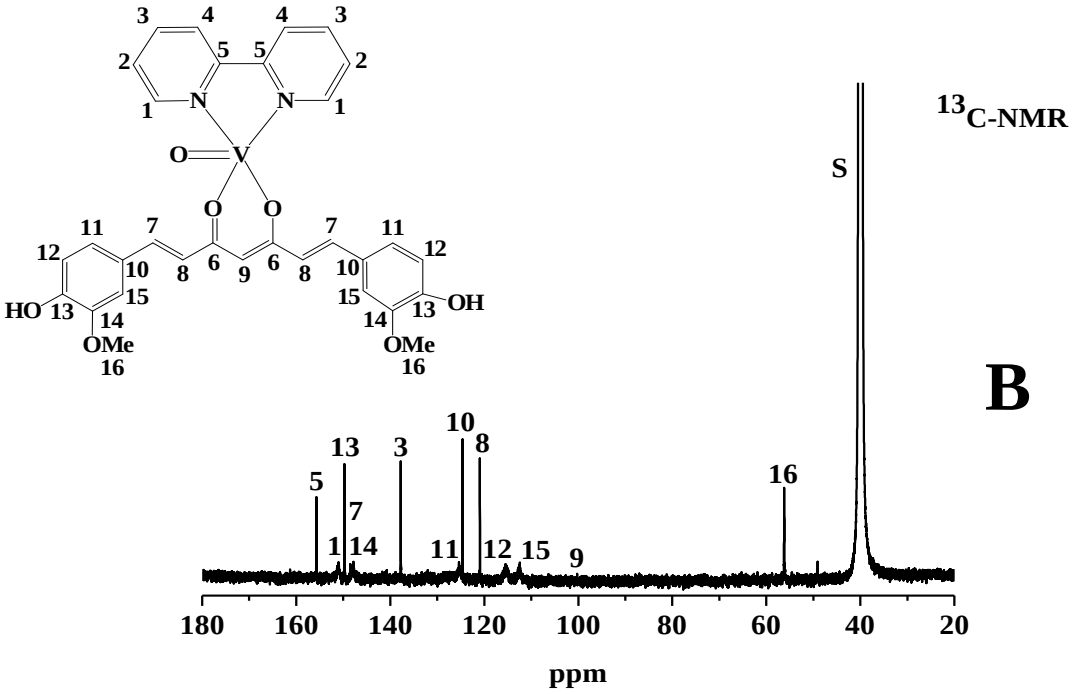
13C-NMR
B
S
10
8
13
3
5
16
7
1
14
11
12
15
9
180
160
140
120
100
80
60
40
20
ppm

Figure 3

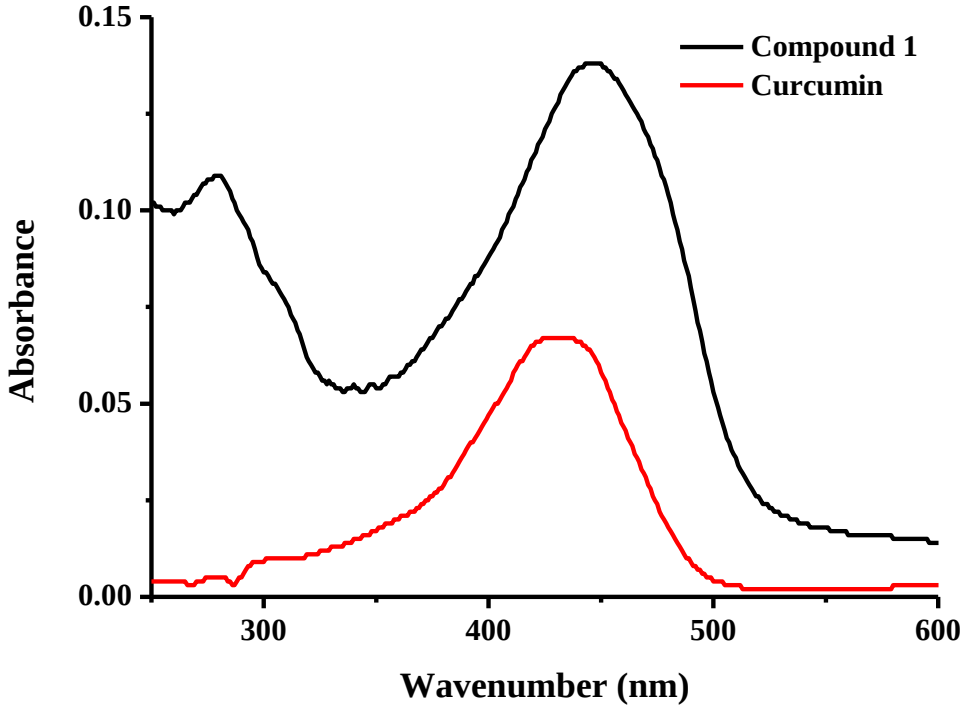
Compound 1
Curcumin
Absorbance
Wavenumber (nm)
0.15
0.10
0.05
0.00
300
400
500
600

A

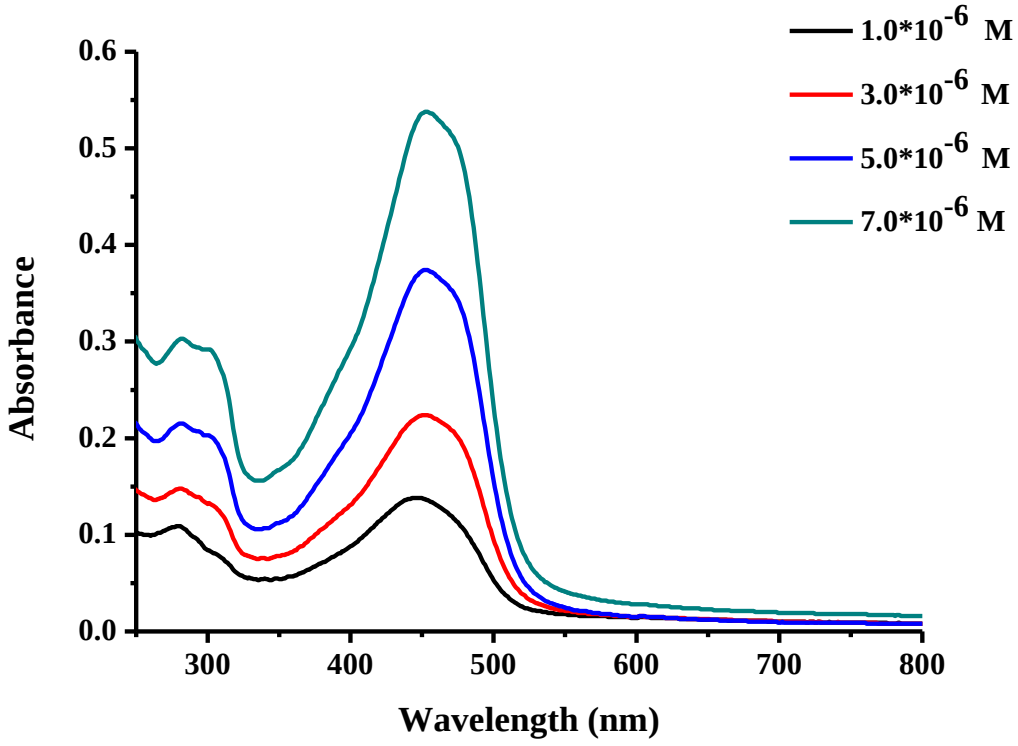
1.0*10-6 M
3.0*10-6 M
5.0*10-6 M
7.0*10-6 M
Absorbance
Wavelength (nm)
0.6
0.5
0.4
0.3
0.2
0.1
0.0
300
400
500
600
700
800

B

Figure 4

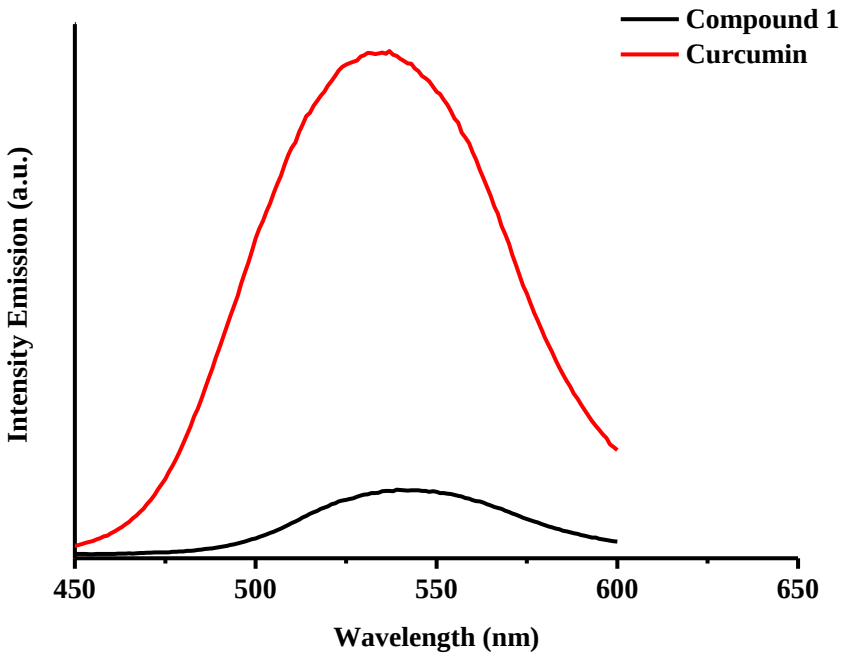

Figure 5

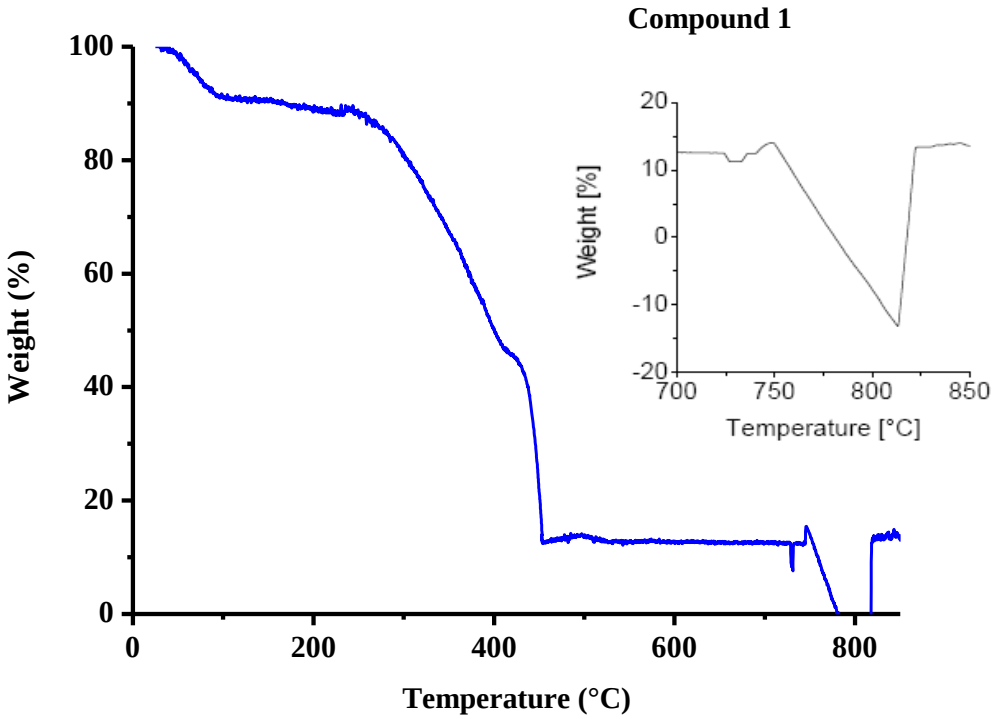

Figure 6

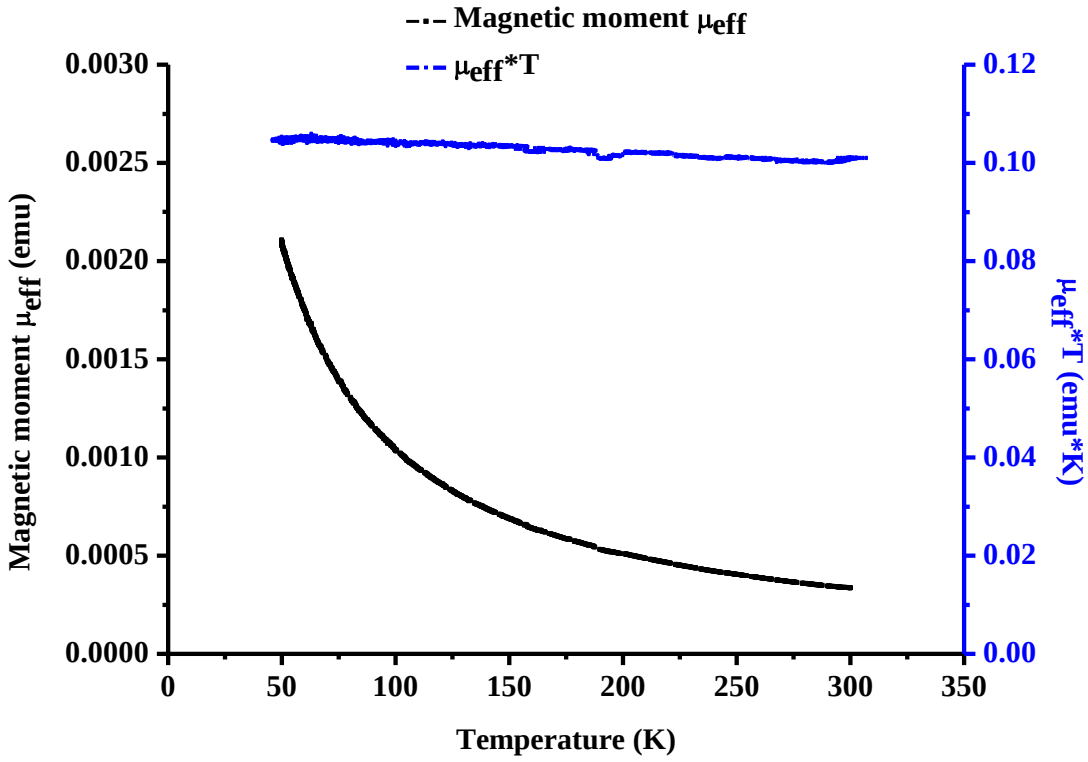

Figure 7

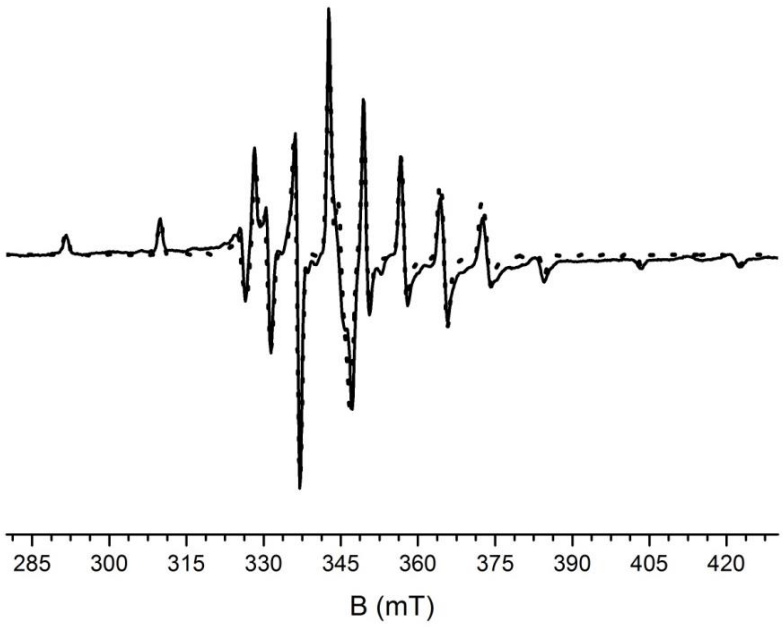

Figure 8

A

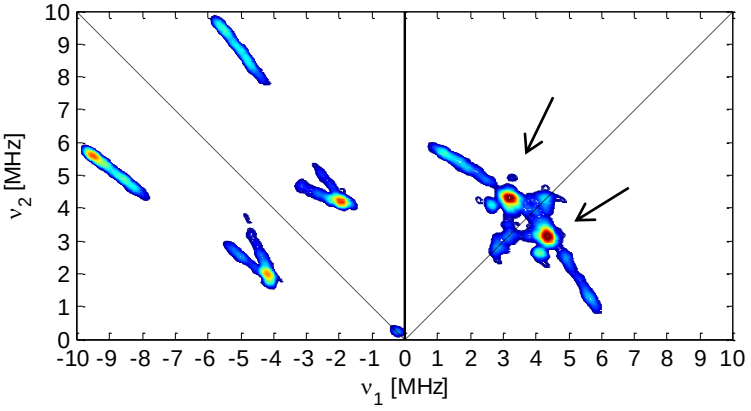

B

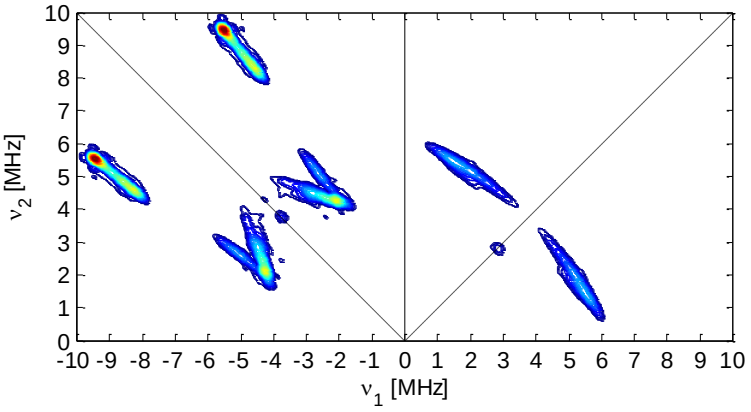

C

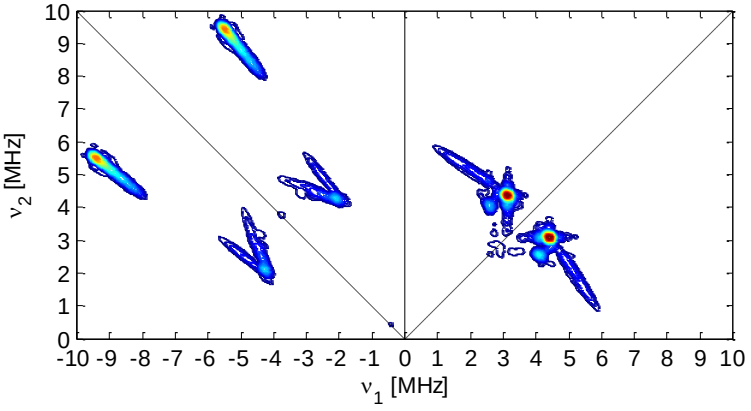

Figure 9

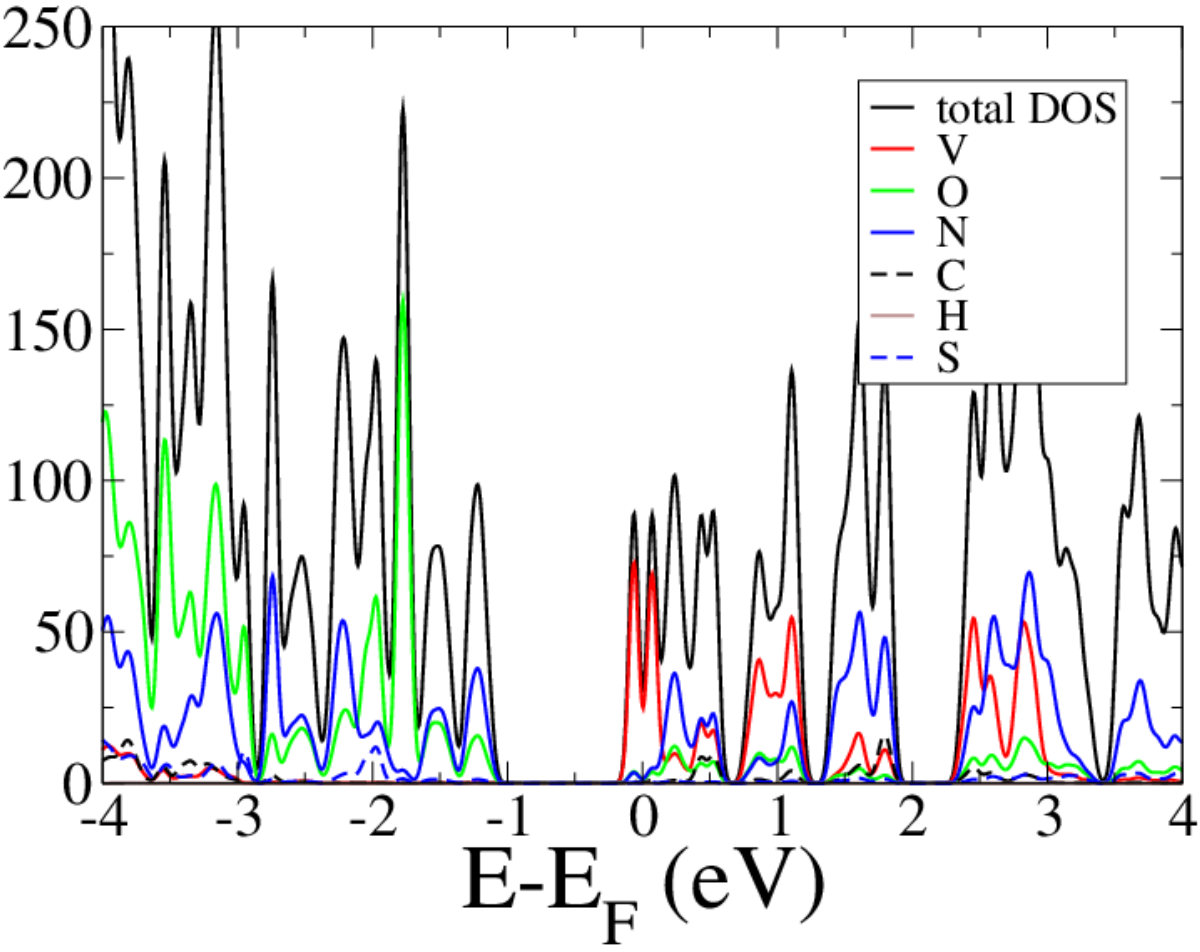

A

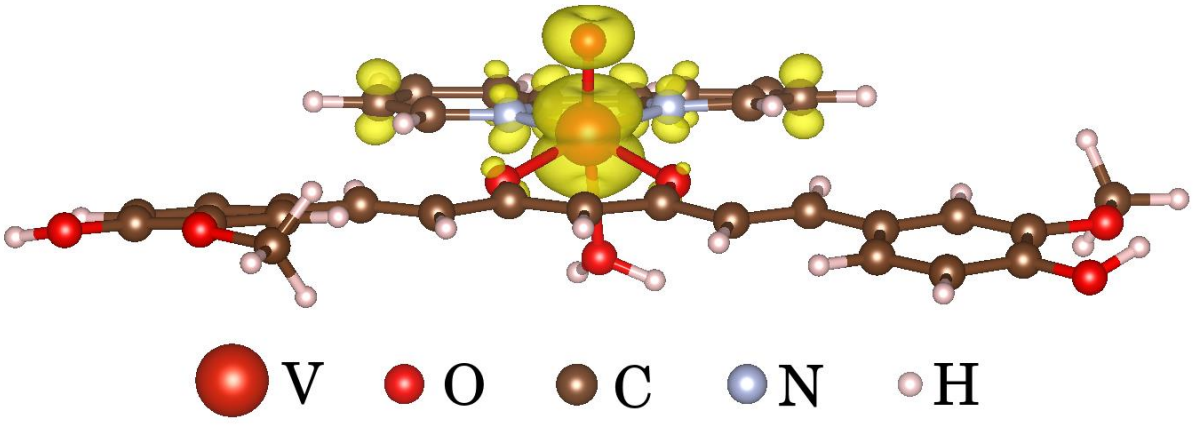

B

Figure 10

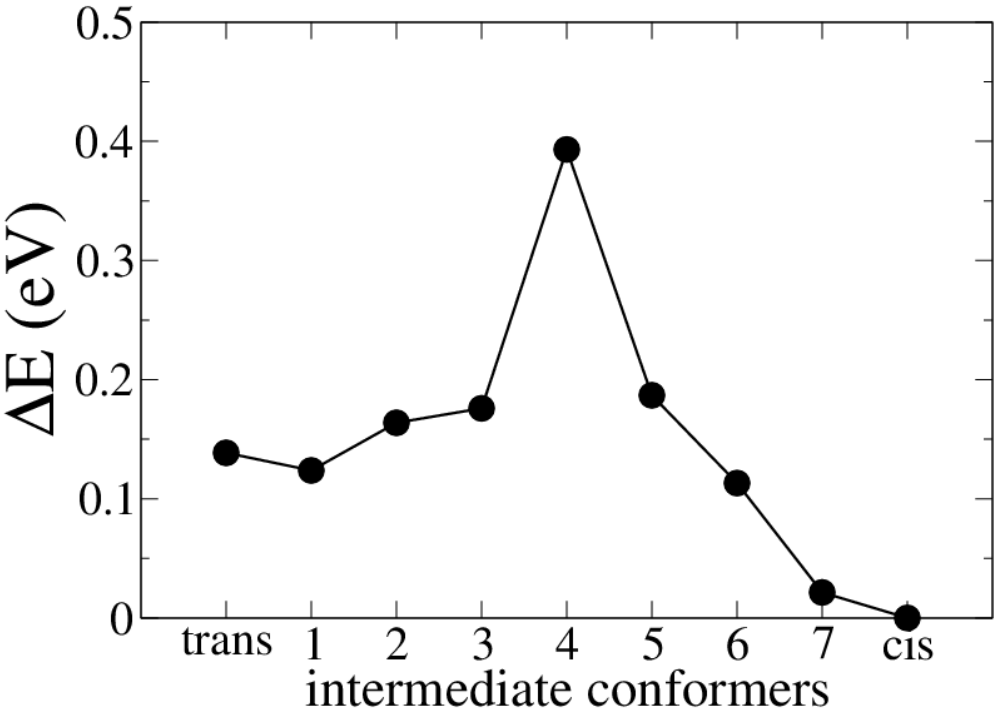

Figure 11

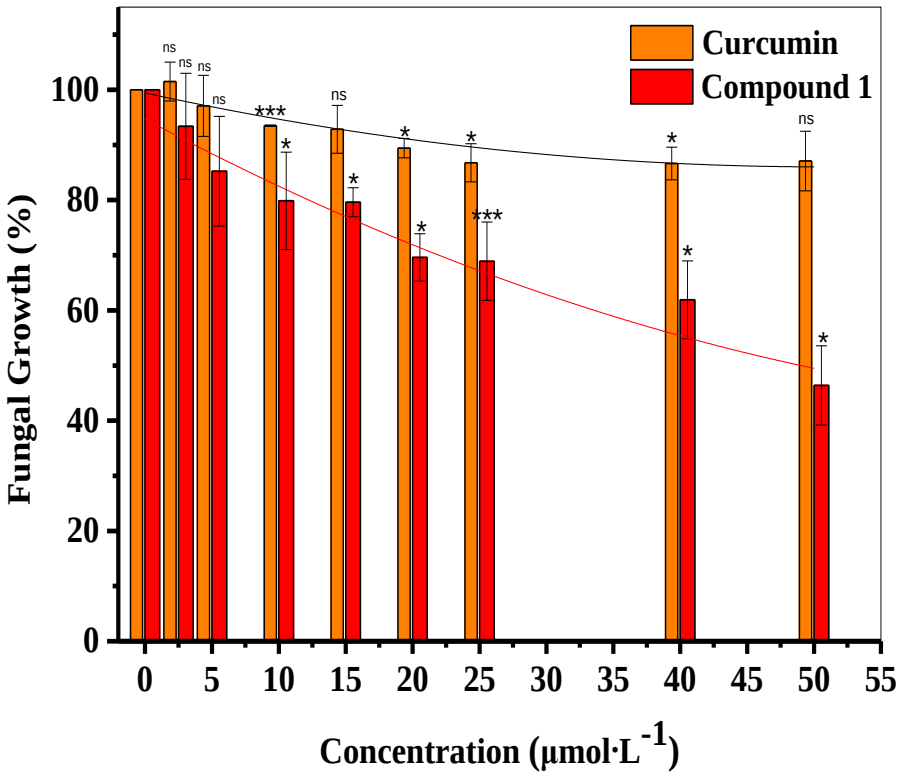

Figure 12

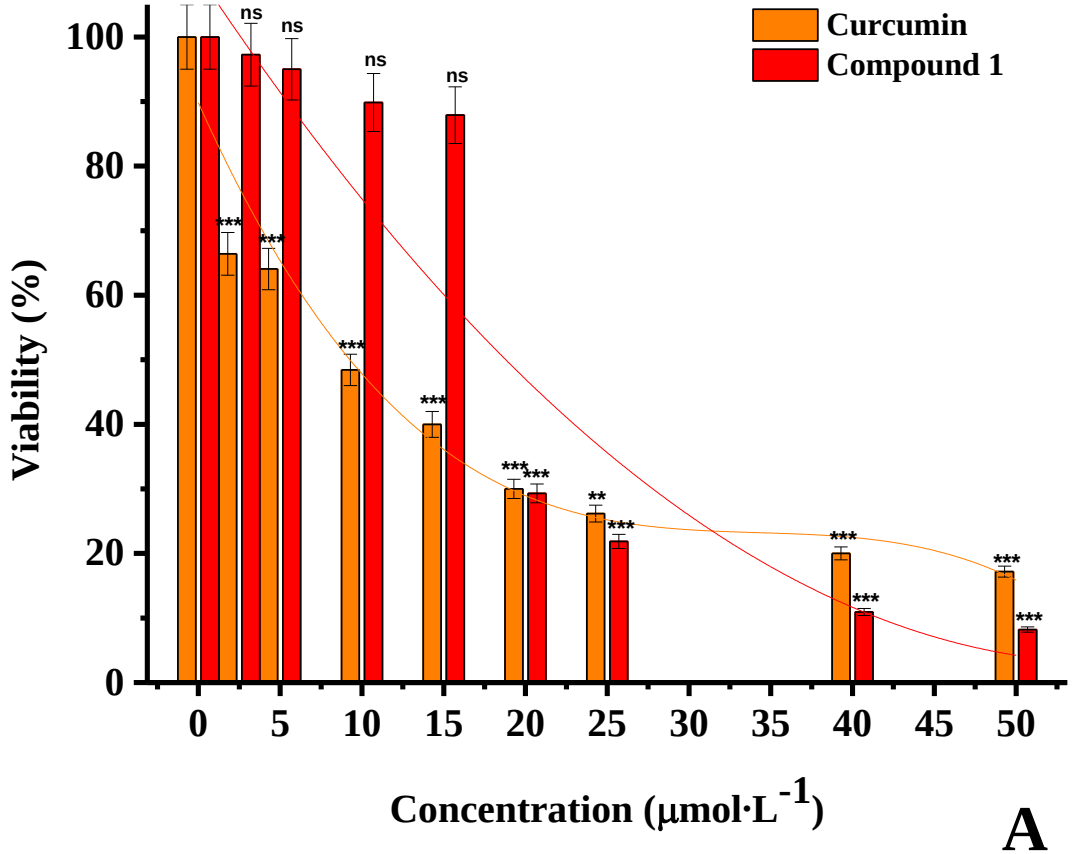
Curcumin
Compound 1
Viability (%)
Concentration (μmol·L-1)
ns
***
**
0
20
40
60
80
100
0
5
10
15
20
25
30
35
40
45
50

A

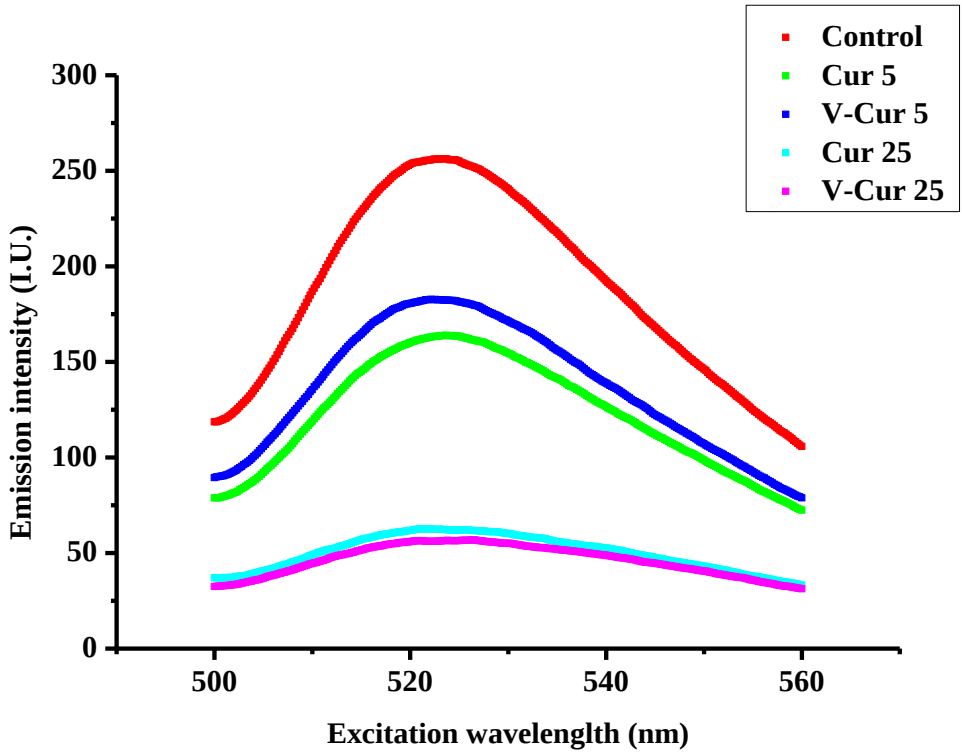
Control
Cur 5
V-Cur 5
Cur 25
V-Cur 25
Emission intensity (I.U.)
Excitation wavelenglth (nm)
0
50
100
150
200
250
300
500
520
540
560

B

Figure 13

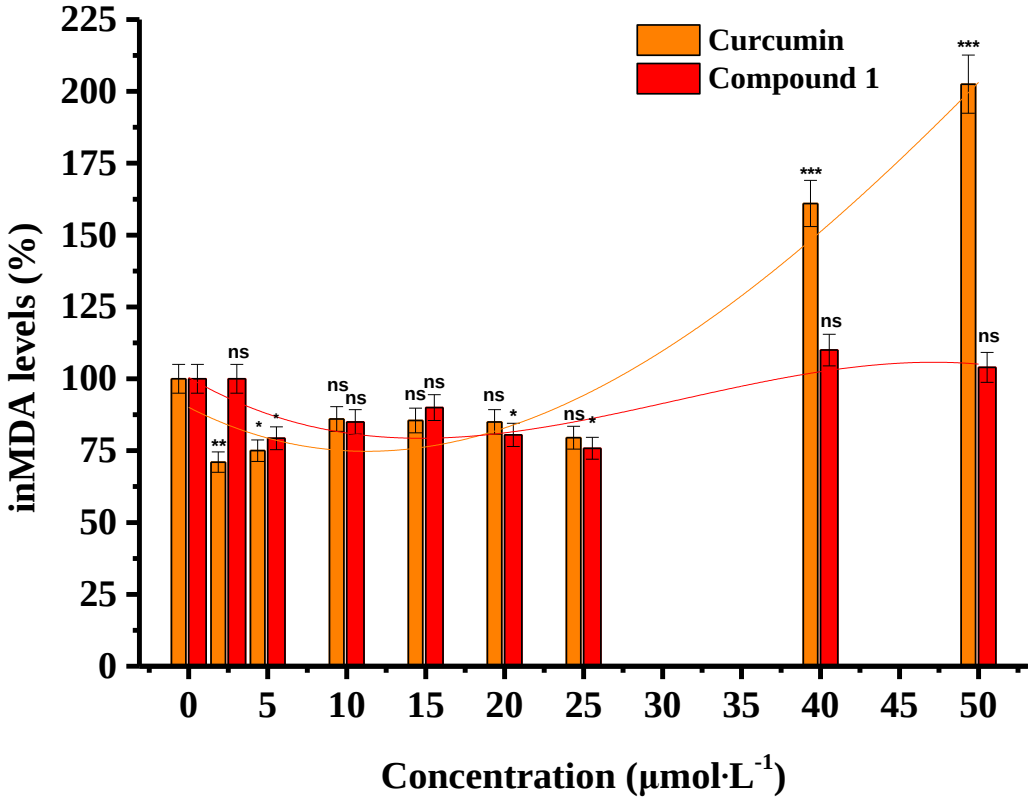
Curcumin
Compound 1
inMDA levels (%)
Concentration (μmol·L-1)
A

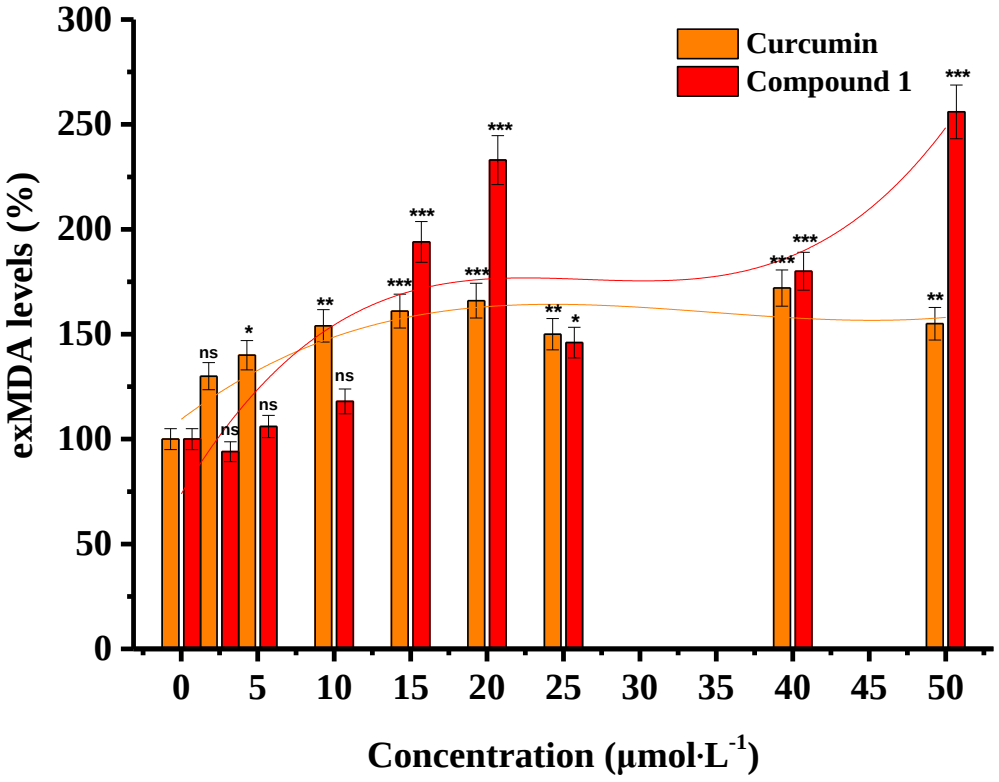
Curcumin
Compound 1
exMDA levels (%)
Concentration (μmol·L-1)
B

Figure 14

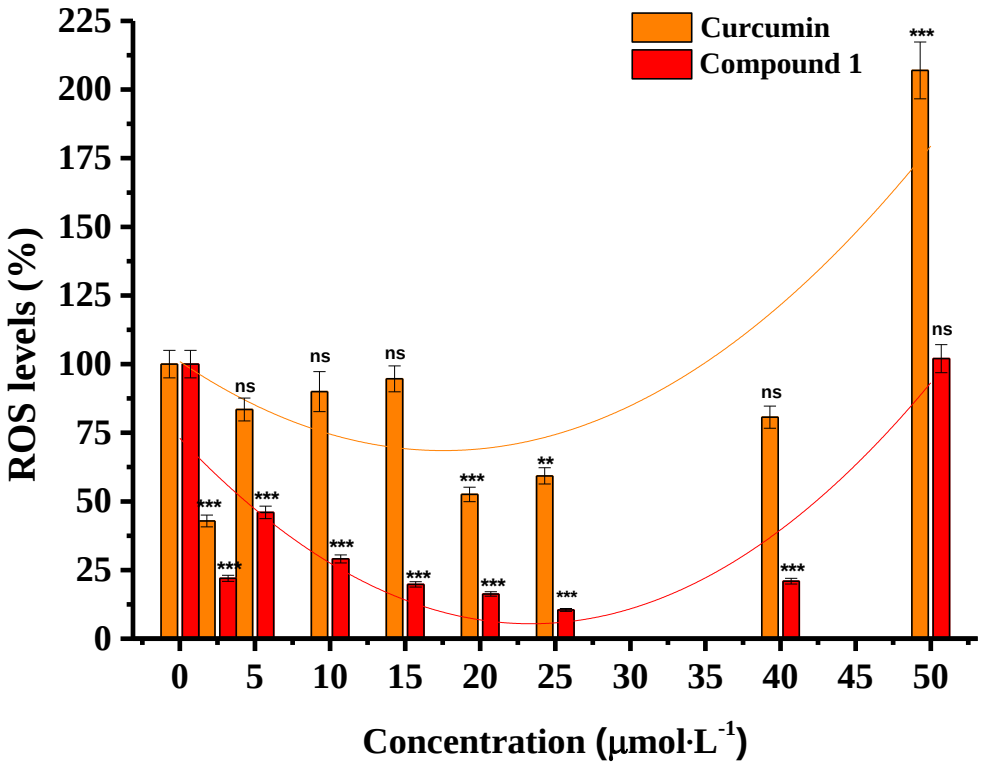
Curcumin
Compound 1
ROS levels (%)
Concentration (μmol·L-1)
0
25
50
75
100
125
150
175
200
225
0
5
10
15
20
25
30
35
40
45
50
ns
***
**

Figure 15

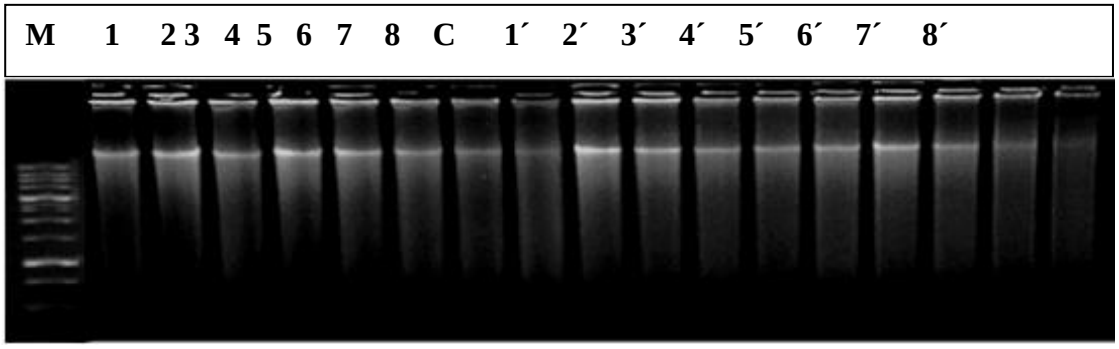

A

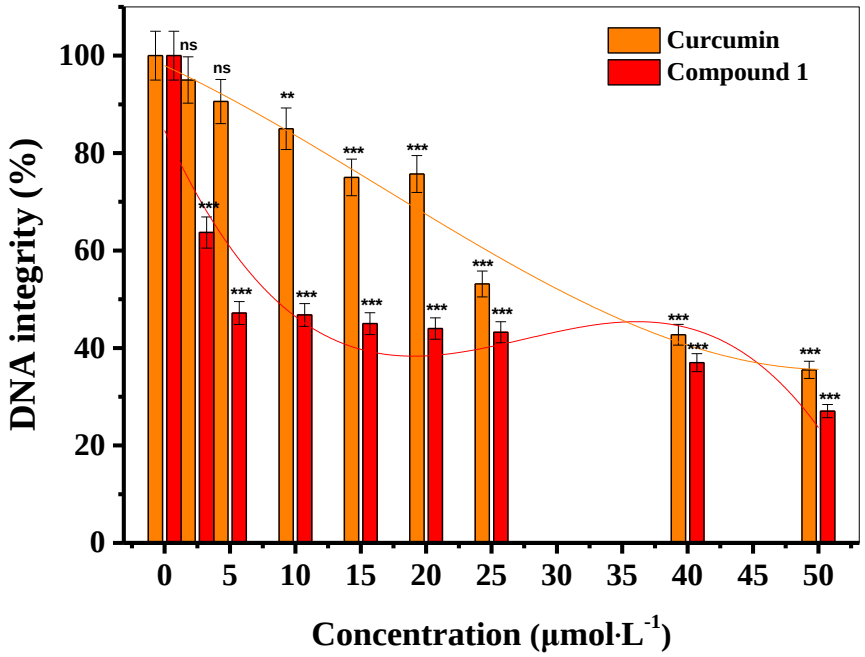

B

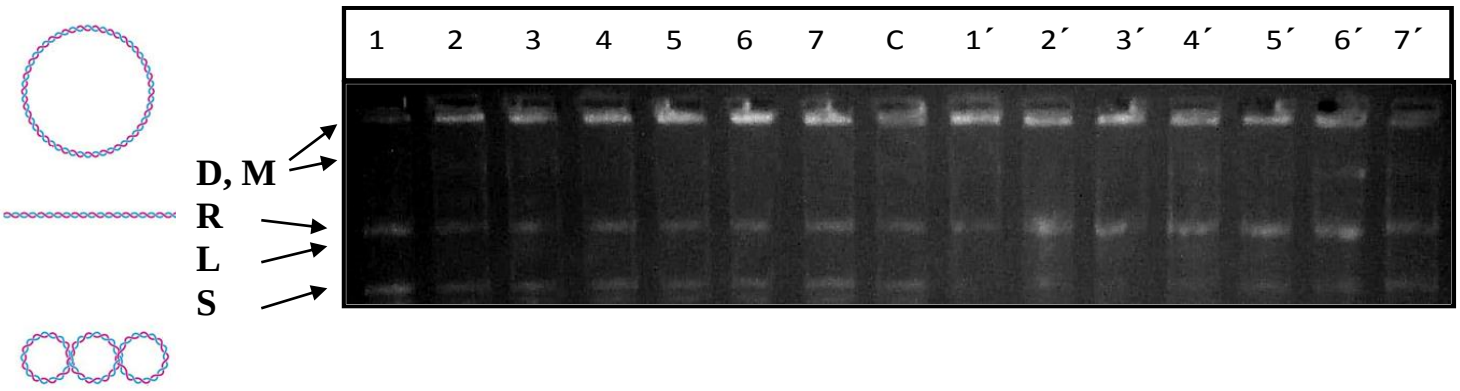

C

Figure 16